MATHEMATICAL BIOSCIENCES
AND ENGINEERING
Volume **2**, Number **1**, January **2005**

http://www.mbejournal.org/

pp. **173–210**

TOWARDS AN INTEGRATED PHYSIOLOGICAL THEORY OF MICROBIAL GROWTH: FROM SUBCELLULAR VARIABLES TO POPULATION DYNAMICS

Atul Narang

Department of Chemical Engineering, University of Florida, Gainesville, FL 32611-6005

Sergei S. Pilyugin

Department of Mathematics, University of Florida, Gainesville, FL 32611-8105

(Communicated by Yang Kuang)

Abstract. The dynamics of microbial growth is a problem of fundamental interest in microbiology, microbial ecology, and biotechnology. The pioneering work of Jacob Monod, served as a starting point for developing a wealth of mathematical models that address different aspects of microbial growth in batch and continuous cultures. A number of phenomenological models have appeared in the literature over the last half century. These models can capture the steady-state behavior of pure and mixed cultures, but fall short of explaining most of the complex *dynamic* phenomena. This is because the onset of these complex dynamics is invariably driven by one or more intracellular variables not accounted for by phenomenological models.

In this paper, we provide an overview of the experimental data, and introduce a different class of mathematical models that can be used to understand microbial growth dynamics. In addition to the standard variables such as the cell and substrate concentrations, these models explicitly include the dynamics of the physiological variables responsible for adaptation of the cells to environmental variations. We present these physiological models in the order of increasing complexity. Thus, we begin with models of single-species growth in environments containing a single growth-limiting substrate, then advance to models of single-species growth in mixed-substrate media, and conclude with models of multiple-species growth in mixed-substrate environments. Throughout the paper, we discuss both the analytical and simulation techniques to illustrate how these models capture and explain various experimental phenomena. Finally, we also present open questions and possible directions for future research that would integrate these models into a global physiological theory of microbial growth.

1. **Introduction.** The growth of microbial species in media containing one or several growth-limiting substrates is of immense importance in ecology and bioengineering. For example, microbes play a vital role in the global carbon cycle. Each year, approximately 50×10^9 tons of carbon is fixed into biomass by autotrophic bacteria in the upper 10 m of the ocean. Some 30% of this fixed carbon enters the grazing food chain that consists of zooplankton and fish. But 50% is rapidly

2000 *Mathematics Subject Classification.* 92D25, 92D37, 92D45.

Key words and phrases. Microbial growth, phenomenological and physiological models, transient dynamics, chemostat, mixed microbial cultures, peripheral enzymes, ribosomes, RNA.

consumed by the microbial loop within the upper layers, and another 20% sinks 10–1000 m below sea level where it is slowly remineralized by heterotrophic bacteria. This "biological pump" is responsible for reducing the atmospheric CO_2 concentration by an estimated 400 ppm [63]. Our ability to understand and combat global warming therefore hinges upon detailed knowledge of the mechanisms that mediate the carbon flux through bacteria. Microbes play an equally important role in bioengineering. Examples of particular interest include

1. *Bioethanol fermentation:* The feedstocks used for bioethanol fermentation typically consist of a mixture of hexoses (primarily glucose) and pentoses (primarily xylose). Bioethanol is the by-product obtained when microbes consume this mixture of hexoses and pentoses.
2. *Bioremediation:* Gasoline and chemical spills generally yield a complex mixture of water-soluble organic compounds. In gasoline spills, for instance, the four compounds of concern are benzene, toluenne, ethylbenzene, and xylene. Bioremediation of gasoline spills involves the consumption of this mixture by microorganisms.
3. *Biopolymer synthesis:* Biopolymers, such as polyhydroxybutyrate, are synthesized by exposing microbes to nitrogen-limited conditions.

Evidently, a deeper understanding of microbial growth has diverse and profound implications.

There is a vast body of work on mathematical models of microbial growth, dominated almost entirely by phenomenological models of growth. These models consider only the substrate and cell concentrations as state variables, and completely ignore the role of intracellular variables. However, in most instances, the microbial response to environmental variations is intimately linked to adaptive changes within the cell. Consider, for instance, the growth of a microbial culture limited by a single substrate. When such a culture is suddenly exposed to substrate-excess conditions, the specific growth rate does not increase immediately. Instead, there is a slow adaptive response, because the cells must first synthesize the enzymes required to metabolize the additional substrate available in the environment. Phenomenological models, such as the Monod model or its many variants, cannot capture these dynamics, since intracellular enzymes are not a part of the description of the model. Not surprisingly, the phenomenological models predict instantaneous recovery in the face of environmental perturbations, whereas the experiments show long recovery times. Another example revealing the inadequacy of phenomenological models is the growth of a microbial species on a mixture of two *substitutable* substrates, i.e. substrates that fulfil the same nutrient requirements, such as two carbon sources or two nitrogen sources. Given these two alternative sources of the same nutrient, microbes often display anthropomorphic choice. They preferentially consume the nutrient source that supports a higher growth rate. It is only after exhaustion of the "preferred" substrate that they begin consuming the "less preferred" substrate. To capture this behavior, the phenomenological models generally assume that the "preferred substrate" somehow inhibits growth on the "less preferred" substrate. But this hypothesis sheds no light on the mechanism by which the inhibition is exerted. It is well known from molecular biology, dating back to the pioneering studies of Monod and his coworkers in the early 60's, that the uptake of the "less preferred" substrate is abolished precisely because the enzymes that catalyze the uptake of this substrate cannot be synthesized in the presence of the "preferred" substrate. Models that ignore the dynamics of these transport enzymes may fit the

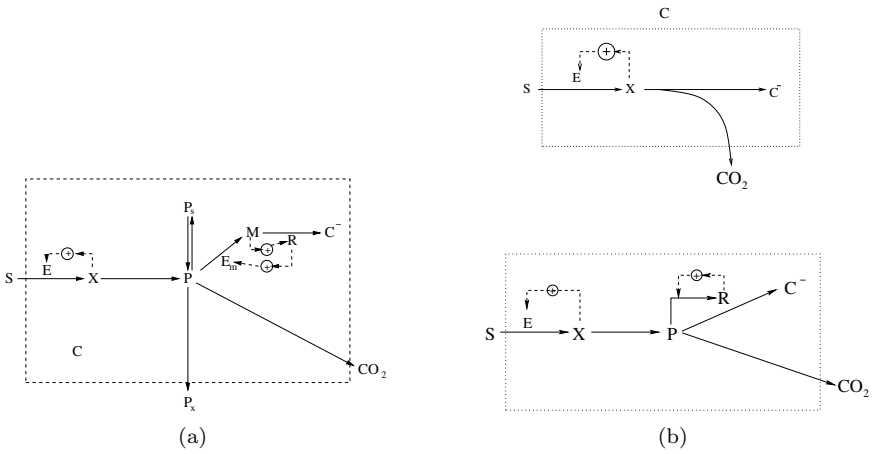

FIGURE 1. (a) General model of microbial growth on a single growth-limiting carbon source. (b) Special cases of the general model used to study the role of peripheral enzymes (top) and ribosomes (bottom). In all the figures, S denotes the carbon and energy source; E denotes the coordinately controlled peripheral enzymes that catalyze the transport and peripheral catabolism of S; X denotes the internalized form of the substrate that induces the synthesis of E; P denotes the pool of precursors produced by catabolism of X; P_s denotes internally stored compounds; P_x denotes excreted metabolites; E_m denotes the biosynthetic enzymes GDH, GOGAT. M is the pool of amino acid monomers; R denotes the ribosomes (or ribosomal RNA); C^- denotes proteins; and C denotes the total biomass of the cells.

data, but they cannot address the central biological question (why is the synthesis of these enzymes inhibited?) without first admitting the transport enzymes as state variables. There is growing recognition among both biologists and mathematicians of the need for physiological models. In a recent commentary [2], it was observed that

> "Because microbes influence ecosystems through molecular interactions, for example, involving cell surface receptors, permeases, or enzymes, ... microbes' ecosystem activities, whether they involve carbon cycling or pathogenesis toward marine animals, should be modeled as molecular events."

We have worked toward this goal for several years. Our modeling efforts have spanned the entire spectrum from dynamics of single-species, single-substrate limited growth to multiple-species, multiple-substrate limited growth. This paper is a summary of our results.

The main obstacle standing in the way of physiological model formulation is identification of the variables. Even the seemingly simple bacterial cell contains several hundred metabolites and enzymes. Which of these variables are important for describing the dynamic response of the system? Our main modeling hypothesis

is that despite the complexity of the metabolic pathways, the dynamics of microbial growth and substrate consumption are governed by a few key intracellular variables, namely, peripheral enzymes, biosynthetic enzymes, ribosomes, and nucleotide phosphates. This hypothesis is based on the belief that only a handful of variables are relevant on the time scale of interest (hours to days) - the "fast" variables rapidly attain quasi steady-state, and the "very slow" variables do not change at all. Indeed, in what follows, we frequently reduce the complexity of the model by appealing to the separation of time scales. But in the final analysis, the most compelling argument supporting our hypothesis is the good agreement between the model simulations and the experimental data.

We begin by considering the simplest case of single-species, single-substrate cultures (section 2). We have used this simple setting to identify the variables by an iterative process involving model formulation and comparison with experiments. The variables thus identified form the foundation upon which we have built models of mixed-substrate and mixed-culture growth (sections 3 and 4). Our models represent only the beginning of an attempt to create a unified physiological theory. In section 5, we discuss several outstanding problems that appear to be ripe for attack by rigorous mathematical approaches.

2. **Single-species, single-substrate cultures.** In the literature, the most popular abstraction of single-substrate growth is the Monod model [32]. It is well known, however, that this model fails to describe the transient response to abrupt changes in the environment [35, 26, 50]. The failure of the model stems from the assumption that the substrate uptake and growth rates instantly adjust to variations of the substrate concentration. In reality, the substrate uptake and growth rates do not adjust until certain "slow" intracellular variables have adapted to the new environment. Thus, a key question for understanding the dynamics of single-species, single-substrate cultures is

> *What are the "slow" intracellular variables that prevent the substrate uptake and growth rates from adjusting instantly, and why is their response so slow?*

Based on a careful analysis of the experimental literature, we have identified three intracellular variables as potential sources of the slow response - the peripheral enzymes, the biosynthetic enzymes, and the ribosomes. Figure 1a, which shows a fairly general abstraction of metabolism, illustrates the role of these variables in the most well-studied example - aerobic growth on a single growth-limiting carbon and energy source S (such as glucose or galactose). The peripheral enzymes (E), which catalyze the peripheral catabolism of the substrate, yield the inducer (X), that induces (stimulates) the synthesis of the peripheral enzymes.[1] Catabolism of X by the central metabolic pathways yields the pool of metabolites or precursors (P). The biosynthetic enzymes (E_m) catalyze the synthesis of amino acid monomers

[1]Peripheral catabolism refers to the transport of the substrate into the cell, and its subsequent chemical modifications before entry into the so-called central metabolic pathways, such as glycolysis or the citric acid cycle. Although it often entails multiple reactions, all the enzymes of peripheral catabolism are, in general, coordinately controlled, i.e., their synthesis rates are coupled because they are transcribed in tandem. Thus, we find it appropriate to "lump" all the peripheral enzymes into a single variable.

(M) from the precursors, and the ribosomes (R) catalyze the synthesis of proteins (C^-) from the monomers. [2]

Our goal is to unravel the relative roles of the three "slow" variables E, E_m, and R. To achieve this goal, we have proceeded by systematically increasing the complexity of the model. Thus far, we have investigated the role of peripheral enzymes [57] and ribosomes [24] by considering the simpler abstractions shown in Figure 1b. These results are summarized below. The future work, which concerns the role of biosynthetic enzymes and energy, is described in Section 5.1.

2.1. **The role of peripheral enzymes.** In some instances, the substrate uptake and growth rates respond slowly because the prevailing peripheral enzyme levels are so small that almost no substrate is transported into the cell, even though the exogenous substrate concentration is very high. This is dramatically illustrated by exposing steady-state chemostat cultures to a *substrate switch*. For example, when the growth-limiting carbon source of a *C. heintzii* culture is switched from glucose to nitrilotriacetic acid (NTA), there is almost no substrate uptake, and hence, no growth for 20 hours (see Figs. 2a,b). The inability of the cells to import NTA can be traced to the virtual absence of NTA-monooxygenase, a peripheral enzyme for NTA (Fig. 2c). This raises the questions

> *Why is the initial peripheral enzyme so low and why does it take the cells so long to build up the peripheral enzyme level?*

In [57], we argued that the answer to both questions is related to the fact that peripheral enzyme synthesis is inducible – it is stimulated only when the cells are exposed to the corresponding substrate in the environment. The molecular mechanism underlying this parsimonious behavior is implicit in Figure 1a. When the substrate appears in the environment, the peripheral enzymes facilitate the uptake of the substrate. The intracellular form of the substrate, X, then induces the synthesis of more peripheral enzyme. It follows that the initial level of NTA-monoxygenase is low because the cells have not been exposed to NTA prior to the switch from glucose to NTA. Furthermore, it takes a long time to build up the peripheral enzyme level because its synthesis is autocatalytic. This is evident from the kinetic scheme – the higher the peripheral enzyme level, the larger the inducer concentration and the peripheral enzyme synthesis rate. Since the initial peripheral enzyme level is low, so is its synthesis rate, and this state of affairs persists until the concentration of the enzyme is built up to sufficiently high levels.

To quantify the foregoing argument, we studied the kinetic scheme shown in Figure 1b (top), which focuses on the inducible nature of peripheral enzyme synthesis. The corresponding mass-balance equations for enzyme-limited growth in a

[2] Although there are many biosynthetic enzymes involved in amino acid synthesis, only one of them, namely, glutamate dehydrogenase, provides the large majority (80%) of the amino acids for protein synthesis. Thus, to a first degree of approximation, it is permissible once again to replace the multitude of biosynthetic enzymes by a single enzyme, E_m.

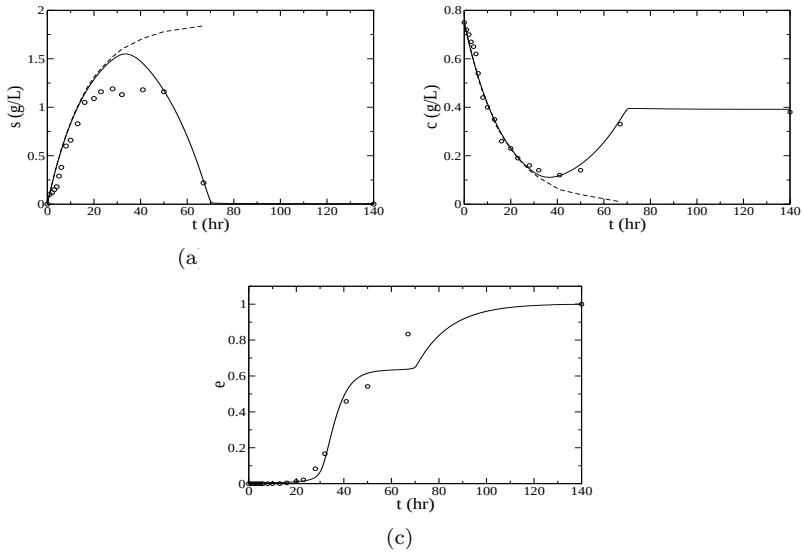

FIGURE 2. Transient response of a *C. heintzii* culture to a switch in the identity of the growth-limiting substrate from glucose to nitrilotriacetic acid (NTA) (data from [4]). The dashed lines in (a) and (b) show the substrate concentrations and cell densities that would be obtained in the absence of any substrate consumption and growth, i.e., $\dot{s} = D(s^f - s)$ and $\dot{c} = -Dc$. The close agreement between the dashed curves and the experimental data implies that there is no perceptible substrate consumption and growth for the first 20 hours. The full lines show the simulations of our model [57]. (a) Concentration of NTA. (b) Cell density. (c) Activity of NTA-monooxygenase scaled such that the maximum activity is 1.

chemostat are

$$\dot{s} = D(s^f - s) - r_s c, \quad r_s \equiv V_s e \frac{s}{K_s + s}, \tag{1}$$

$$\dot{e} = r_e^+ - r_e^- - r_g e, \quad r_e^+ \equiv V_e \frac{1 + K_1 x + K_2 x^2}{K_3 + K_1 x + K_2 x^2}\,,\ r_e^- \equiv k_e^- e, \tag{2}$$

$$\dot{x} = r_s - r_x - r_g x, \quad r_x = k_x x, \tag{3}$$

$$\dot{c}^- = Y r_x - r_g c^-, \tag{4}$$

$$\dot{c} = (r_g - D)c, \tag{5}$$

where D and s^f denote the dilution rate and the substrate concentration in the feed. [3] In equations (1–5), it is assumed that

[3]The variables e, x, and c^- represent the mass-fractions of the peripheral enzymes, inducer molecules, and the rest of the cell biomass so that $e + x + c^- = 1$. For instance, the total concentration of peripheral enzymes in the chemostat is given by ec, et cetera. Hence, the specific growth rate r_g in (2–4) corresponds to the rate at which these mass-fractions are "diluted" due to cell growth. The dilution rate D does not appear in (2–4) because the washout of entire cells has no effect on the internal cell composition.

(a) The specific substrate uptake rate, r_s, is jointly proportional to the peripheral enzyme level and the extent to which it is saturated with the substrate;
(b) The specific peripheral enzyme synthesis rate, r_e^+, is a saturable function of the inducer concentration,[4] and the specific enzyme degradation rate, r_e^-, is proportional to the enzyme level;
(c) The cell biomass growth rate is proportional to the catabolic rate, r_x, with a constant of proportionality, Y, which corresponds to the yield of biomass on the substrate;
(d) The specific catabolic rate, $k_x >> r_g$ is so rapid that the inducer rapidly attains a quasi-steady state. At such quasi-steady state, $x = \frac{r_s}{k_x + r_g} \approx \frac{r_s}{k_x}$, or equivalently, $r_s \approx r_x$.

The quasi-steady state assumption allows to reduce equations (1–5) as follows. Since $e + x + c^- = 1$, we have

$$0 = \dot{e} + \dot{x} + \dot{c}^- = Y r_x - r_x + r_s - r_g,$$

hence the specific growth rate r_g can be expressed as $r_g = Y r_x - r_x + r_s \approx Y r_s = Y V_s e \frac{s}{K_s + s}$. The reduced model then takes the following form

$$\dot{s} = D(s^f - s) - V_s e \frac{s}{K_s + s} c, \tag{6}$$

$$\dot{e} = r_e^+ - k_e^- e - r_g e, \quad r_e^+ \equiv V_e \frac{1 + K_1 x + K_2 x^2}{K_3 + K_1 x + K_2 x^2}, \tag{7}$$

$$x = \frac{V_s e\ s}{k_x (K_s + s)}, \tag{8}$$

$$\dot{c} = \Big(Y V_s e \frac{s}{K_s + s} - D \Big) c. \tag{9}$$

As shown in Figure 2, simulations of the model are in quantitative agreement with the experimental data. At the heart of this agreement is the fact that *peripheral enzyme synthesis is autocatalytic.* An intuitive argument supporting this claim was given above. It is manifested much more clearly in the model. Indeed, substituting (8) in the expression for r_e^+ yields

$$r_e^+ = V_e \frac{1 + K_1' e + K_2' e^2}{K_3 + K_1' e + K_2' e^2}, \quad K_1' \equiv K_1 \left(\frac{V_s}{k_x} \frac{s}{K_s + s} \right), \ K_2' \equiv K_2 \left(\frac{V_s}{k_x} \frac{s}{K_s + s} \right)^2,$$

which shows that the peripheral enzyme synthesis rate is indeed an increasing function of the enzyme level. In the next section, we show that the autocatalytic kinetics of peripheral enzyme synthesis also plays a crucial role in mixed-substrate cultures.

We presented a detailed bifurcation and stability analysis of the model (6–9) in [57]. It is worth mentioning here that the dynamics of (6–9) is essentially two-dimensional due to a conservation law resulting from the constancy of the yield coefficient. Indeed, letting $z = Y s + c$, it is easily seen that $\dot{z} = D(Y s_f - z)$. Hence,

[4]These kinetics are based on the molecular mechanism of induction in the *lac* operon. The coefficients K_1 and K_2 denote the equilibrium constants for binding of one and two inducer molecules to the repressor, and K_3 denotes the equilibrium constant for binding of the repressor to the operator. Note that the enzyme is synthesized at a small rate even in the absence of the inducer ($r_e^+\big|_{x=0} = V_e/K_3 > 0$). This rate corresponds to the constitutive enzyme synthesis.

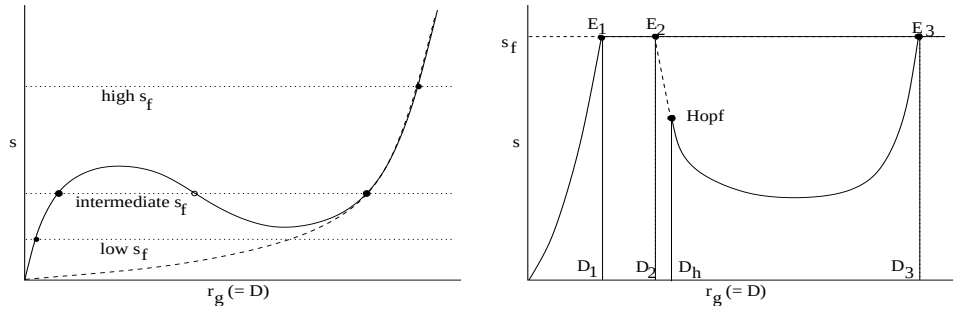

FIGURE 3. (a) Variation of the steady state substrate concentration with respect to the dilution rate (equivalently, the growth rate). The solid line corresponds to the model (6–9). For comparison, the dashed line shows the same graph for the Monod model. The variation of the washout equilibria with respect to s_f can be traced graphically by moving the line $s = s_f$ up or down. For instance, for high or low values of s_f, the washout equilibrium is unique. For intermediate values of s_f, the model admits three washout equilibria. (b) The bifurcation diagram of (6–9) for intermediate values of s_f corresponds to the part of (a) that lies below $s = s_f$. The washout occurs at both high ($D = D_3$) and low ($D = D_2$) values of the dilution rate. The Hopf bifurcation at $D = D_h$ indicates the onset of sustained oscillations. We should point out that the middle washout steady-state E_2 is always unstable, while the stability of E_1 and E_3 changes with D. We point out that this bifurcation diagram can be equivalently replotted in terms of $c = Y(s_f - s)$.

(6–9) can be further reduced to the limiting system

$$\dot{s} = (s^f - s)(D - r_g), \quad r_g \equiv YV_s e \frac{s}{K_s + s} \tag{10}$$

$$\dot{e} = r_e^+ - (k_e^- + r_g)e, \quad r_e^+ \equiv V_e \frac{1 + K_1 x + K_2 x^2}{K_3 + K_1 x + K_2 x^2},\ x \equiv \frac{r_g}{Y k_x}. \tag{11}$$

Note that the line $s = s_f$ is an invariant set of (10–11) that corresponds to the microbial washout ($c = 0$). At the persistence steady state, we have $s < s_f$ and $r_g = D$. Substituting $\dot{e} = 0$ into (11), we can express the steady-state values $e = e(D)$ and $s = s(D)$ as functions of the dilution rate D. Figure 3a shows the graph of $s = s(D)$ for the biologically reasonable range of parameters (for details, see [57]). The part of the graph that lies above the line $s = s_f$ corresponds to the microbial washout and each intersection $s(D) = s_f$ corresponds to a transcritical bifurcation of a washout equilibrium. For intermediate values of the feed concentration s_f, there are three intersections and thus three distinct washout equilibria E_1, E_2, E_3 as shown in Figure 3b. One particularly important property of the model (6–9) is the existence of a minimal growth rate (shown as D_2 in Fig. 3b). Specifically, for intermediate values of s_f, the washout occurs at both high and low dilution rates. Interestingly, this feature is commonly observed in the experimental literature.

If we treat the dilution rate D as a bifurcation parameter, then Figure 3b can be interpreted as the bifurcation diagram of (10–11). Transcritical bifurcations corresponding to the washout occur at three values $D = D_i,\ i = 1, 2, 3$. The persistence steady state exists for $D \in (0, D_1) \bigcup (D_2, D_3)$. The stability of the persistence steady state is determined by the variational matrix J with

$$\mathrm{tr}J = \frac{\partial r_e^+}{\partial e} - 2D - k_e^- - (s_f - s)\frac{\partial r_g}{\partial s}, \quad \det J = (s^f - s)\frac{\partial r_g}{\partial s}(D + k_e^-).$$

In [57], we demonstrated that $\mathrm{tr}J$ is positive at $D = D_2$ and negative at $D = D_3$, whereas $\det J$ remains positive for all $D_2 < D < D_3$. Due to continuity, $\mathrm{tr}J$ changes sign at some intermediate value $D_h \in (D_2, D_3)$ corresponding to a Hopf bifurcation. The persistence steady-state is stable for $D > D_h$ and unstable for $D < D_h$. We also showed that a Hopf bifurcation may occur even if E_2 does not exist (for details, see [57]) hence, the existence of E_2 is sufficient but not necessary for a Hopf bifurcation.

2.2. **The role of ribosomes.** The peripheral enzymes, which form the basis of the model discussed above, are not the sole source of the slow physiological response to substrate-excess conditions. This is evident from experiments in which a chemostat is subjected to dilution rate shift-ups. Figure 4 (upper panel) shows that when a glucose-limited culture of *E. coli* is subjected to a dilution rate shift-up from $D_0 = 0.2$ 1/hr to $D = 0.6$ 1/hr, the substrate concentration attains supersaturating levels within 30 minutes (Fig. 4a), but the specific growth rate does not attain its final value of 0.6 1/hr until 5 hours have elapsed (Fig. 4c). This is similar to the transient shown in Figure 2. However, the slow response here is due to a limitation in the RNA/protein synthesis rate rather than the substrate uptake rate. This is forcefully revealed by the initial response to continuous-to-batch shifts. In these experiments, cells maintained at steady state in a chemostat are abruptly exposed to excess substrate concentrations, and the initial rates of various processes are measured within 10–15 minutes of the exposure. The experiments show that the specific substrate uptake rate rapidly increases to the maximal levels obtained near the washout dilution rate (Fig. 5a). However, the specific rate of RNA and protein synthesis increases only partially if the culture has been growing at low dilution rates, and does not increase at all if the culture has been growing at high dilution rates (Fig. 5b). It follows that when cells growing at steady state in a chemostat are exposed to substrate-excess conditions, the substrate enters the cell at near-maximal rates, but the catabolic products derived from it are, at best, only partially channeled into RNA and protein synthesis. The excess substrate, which accumulates within the cell in the form of precursors, is instantly eliminated by rapidly increasing the rates of respiration (Fig. 5c), excretion (Fig. 5d), and storage [28, 59].

The initial response of continuous-to-batch shifts reveals the identity of the processes that prevent the growth rate from increasing instantly, but sheds no light on the reason for their slow response. We gain some insight into the mechanism of the slow response by examining the *entire* response of glutamate dehydrogenase (GDH) and ribosome levels in continuous-to-batch shifts (Figs. 5e,f). These transients suggest that synthesis of GDH and ribosomes is autocatalytic. Their synthesis rates are small initially, accelerate subsequently, and subside finally after passing through an inflection point. It is conceivable that these autocatalytic kinetics occur because of the positive feedback loop shown in Figure 1a. An increase in the activity of

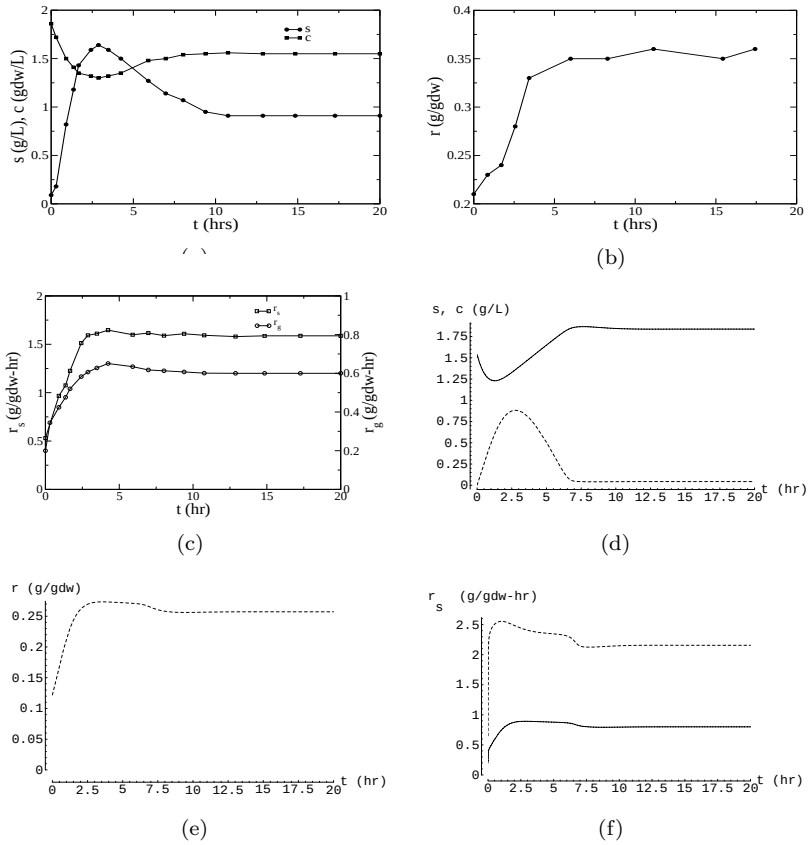

FIGURE 4. Transient response to dilution rate shifts . The upper panel shows the response of a glucose-limited culture of *E. coli* K12 to a shift-up from $D_0 = 0.2$ 1/hr to $D = 0.6$ 1/hr (from [65]). The lower panel shows a simulation of the response to a shift-up from $D_0 = 0.2$ 1/hr to $D = 0.8$ 1/hr (from [24]). The figures show the evolution of (a,d) the cell density and substrate concentration, (b,e) the RNA level, and (c,f) the specific growth and substrate uptake rates.

GDH results in elevated amino acid levels. Amino acids stimulate the synthesis of ribosomal RNA and ribosomes [8, 33, 67], which, in turn, stimulates the synthesis of even more GDH.

To capture these dynamics, we assumed as a starting point that the biosynthetic enzyme, E_m, is in excess so that protein synthesis is limited by ribosomes, and synthesis of ribosomes is autocatalytic [Figure 1b (bottom)]. This led to the

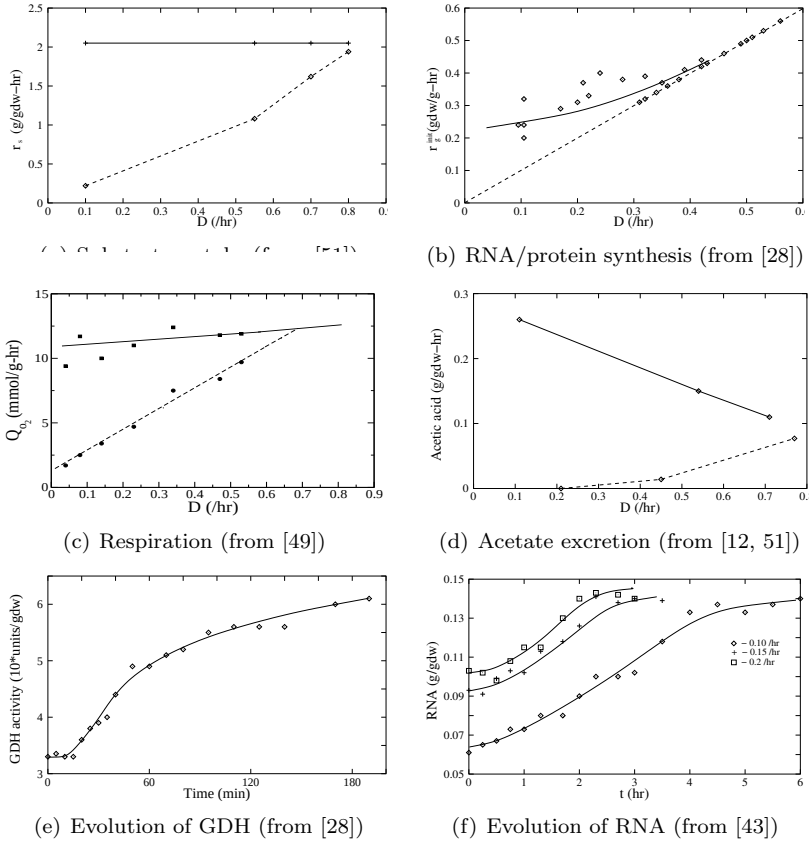

(b) RNA/protein synthesis (from [28])

(c) Respiration (from [49])

(d) Acetate excretion (from [12, 51])

(e) Evolution of GDH (from [28])

(f) Evolution of RNA (from [43])

FIGURE 5. (a,b,c,d) Initial response of glucose-limited steady-state continuous cultures to saturating concentrations of glucose. The dashed line shows the rate of a process when the culture is in steady state at a particular dilution rate. The full line shows the rate of the same process immediately after the steady-state culture has been exposed to saturating concentrations of glucose. The data in (b) was obtained with glycogenless mutants of *E. coli* B at 30℃. All other data was obtained with wild-type *K. aerogenes* at 37℃. (e,f) The dynamic response of GDH and RNA in glucose-limited cultures subjected to continuous-to-batch shifts: The evolution of both GDH activity and RNA levels has a sigmoidal profile. The three curves in (f) correspond to three different dilution rates.

equations [24]

$$\dot{s} = D(s_f - s) - r_s c, \quad r_s \equiv V_s e \frac{s}{K_s + s}, \tag{12}$$

$$\dot{c} = (r_g - D)c, \quad r_g \equiv r_s - r_{\mathrm{co}_2},\ r_{\mathrm{co}_2} \equiv k_{\mathrm{co}_2} p, \tag{13}$$

$$\dot{c^-} = r_c^+ - r_c^- - r_g c^-, \quad r_c^+ \equiv V_c r \frac{p}{K_c + p},\ r_c^- \equiv k_c^- c^-, \tag{14}$$

$$\dot{e} = r_e^+ - r_e^- - r_g e, \quad r_e^+ \equiv V_e \frac{r}{K_e + r} \frac{1 + K_1 x + K_2 x^2}{K_3 + K_1 x + K_2 x^2},\ r_e^- \equiv k_e^- e, \tag{15}$$

$$\dot{r} = r_r^+ - r_r^- - r_g r, \quad r_r^+ \equiv k_r^+ r \bar{p},\ r_r^- \equiv k_r^- r, \tag{16}$$

$$\dot{x} = r_s - r_x - r_g x, \quad r_x \equiv k_x x, \tag{17}$$

$$\dot{p} = r_x - r_{\mathrm{co}_2} - (r_c^+ - r_c^-) - (r_e^+ - r_e^-) - (r_r^+ - r_r^-) - r_g p, \tag{18}$$

where we assumed that
(a) The expression for r_e^+ reflects the fact that the specific enzyme synthesis rate depends not only on the concentration of the inducer (which stimulates the *transcription* of the gene into the mRNA corresponding to the enzyme), but also on the concentration of ribosomes (which *translate* the mRNA produced by transcription into the string of amino acids corresponding to the enzyme);
(b) The specific protein synthesis rate, r_c^+, is jointly proportional to the catalyst (ribosome) level and the availability of "raw materials" (p) required for synthesizing protein;
(c) The specific RNA synthesis rate, r_r^+, is proportional to p and r, where the dependence on r reflects our assumption that RNA synthesis is autocatalytic;
(d) Degradation of proteins and RNA is a first-order process.

In Appendix A, we reduce equations (12–18) assuming that both inducer and precursor rapidly achieve a quasi-steady state and that the the cell biomass consists almost entirely of ribosomes and proteins ($e,\ x,\ p \ll 1$ and $r+c^- \approx 1$). The reduced system is

$$\begin{aligned}
\dot{s} &= D(s_f - s) - r_s c, && (19)\\
\dot{e} &= r_e^+ - r_e^- - r_g e, && (20)\\
\dot{r} &= r_r^+ - r_r^- - r_g r, && (21)\\
\dot{c} &= (r_g - D)\, c, && (22)\\
0 &\approx r_s - r_x, && (23)\\
r_g &\approx r_x - r_{\mathrm{co}_2}, && (24)\\
r_g &\approx (r_r^+ - r_r^-) + (r_c^+ - r_c^-). && (25)
\end{aligned}$$

Equation (25) shows that the specific growth rate of the cells effectively equals the net rate of synthesis of the major macromolecules in the cell, namely, RNA and proteins.

In [24], we have demonstrated that simulations of the model (19–25) capture the dynamics observed in response to a wide variety of perturbations including continuous-to-batch shifts, dilution rate shifts, and substrate switches (see, for instance, Fig. 4). Here, it will suffice to explain the slow response to dilution rate shift-ups in terms of the model. In dilution rate shift-up, the cells are already growing on the growth-limiting substrate in question, so that the peripheral enzyme level is relatively high. Consequently, immediately after the shift-up, the specific substrate uptake rate jumps to maximal levels, resulting in the accumulation of precursors. This saturates the protein synthesis rate ($r_c^+ \approx V_c r$), so that the protein synthesis cannot increase until the ribosomes are built up to sufficiently high levels. Since synthesis of ribosomes is autocatalytic, it takes a few hours for the RNA and protein synthesis rates (and, hence, the specific growth rate) to increase to the higher level consistent with the new dilution rate.

At first glance, it may seem that the large number of variables in (19–25) precludes the possibility of useful mathematical analysis. Upon closer inspection, however, it becomes clear that further reduction of the equations is feasible, and that this simplification yields deeper insights into the transients. This reduction is obtained by observing that the saturation constant (K_s) is quite small ($\sim$0.001–0.01 g/L), but the substrate supply rate (Ds_f) and the substrate consumption rate ($r_s c$) are both on the order of 0.1–1 g/L-hr. Hence, the substrate concentration switches from saturating levels ($s \gg K_s$) to subsaturating levels ($s \ll K_s$) on a

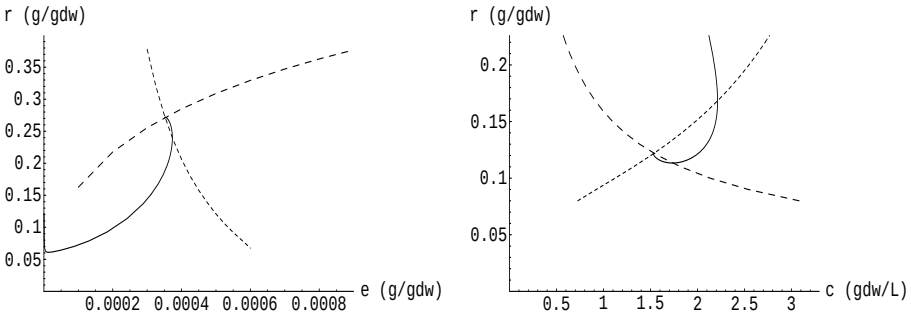

(a) (b)

FIGURE 6. The orbits of the slow motions corresponding to a substrate switch at $D = 0.2$ 1/hr [24]. (a) The slow motion towards balanced growth during substrate-excess conditions ($s \gg K_s$). The line with short dashes shows the nullcline for e; the line with long dashes shows the nullcline for r; the intersection of the two nullclines represents the concentration of e and r at balanced growth; the full line shows the approach of e and r toward the state of balanced growth. (b) The slow motion during substrate-deficient conditions ($s \ll K_s$). The line with short dashes shows the nullcline for c; the line with long dashes shows the nullcline for r; the intersection of the two nullclines represents the steady-state concentrations of c and r at $D = 0.2$ 1/hr; and the full line shows the motion of c and r from balanced growth toward the final steady state.

fast time scale of seconds to minutes. Since the transients typically occur on a time scale of hours, we may say that during a transient, the substrate is either saturating or subsaturating, and the nearly discontinuous transition between these two conditions can be neglected without much loss of accuracy. This is vividly revealed by the data in Figure 2. The substrate concentration almost instantly increases to supersaturating levels, then remains so for the next 70 hrs, at which point it almost instantly switches to subsaturating levels. Thus, a transient can be decomposed into separate time intervals during which the substrate concentration is either saturating or subsaturating. As we show below, the motion during these two limiting conditions can be studied by examining a reduced system of equations.

If the substrate concentration is saturating ($s \gg K_s$), the interior of the cells "sees" a constant environment even if the substrate concentration is changing. Given this quasi-constant environment, the physiological variables move toward a stationary state. Now, the "fast" physiological variables, x and p, are always in a quasi-steady state. The dynamics under substrate-excess conditions is therefore determined by the "slow" motion of e and r toward their stationary state. This slow motion can be analyzed by studying the two-dimensional system of equations obtained by solving (23–24) for $\bar{x}$ and $\bar{p}$ under the constraint $s/(K_s + s) \approx 1$, and substituting these quasi-steady concentrations in (20–21). We refer to this motion as substrate-excess batch dynamics, since this is precisely the motion exhibited by

an inoculum introduced into a batch reactor containing a high substrate concentration. In the face of the quasi steady environment corresponding to the high substrate concentration, the physiological variables of the inoculum move toward a steady state. The attainment of this physiological steady state marks the beginning of exponential or balanced growth. Figure 6a shows that during the approach to balanced growth, the orbit intersects the nullcline for E before intersecting the nullcline for R. It follows that e reaches a maximum before r.

If the substrate concentration is subsaturating ($s \ll K_s$), the substrate concentration is so small that all the substrate entering the reactor is consumed as soon as it enters the reactor. Hence,

$$0 = D(s_f - s) - r_s c \quad \Rightarrow \quad r_s \approx \frac{D s_f}{c},$$

i.e., the specific substrate uptake rate is independent of the enzyme level. Now, $\bar{p}$ feels the effect of the peripheral enzyme level through the specific substrate uptake rate [see equations (23–24)]. Since r_s is independent of the enzyme level, so is the quasi-steady state precursor level, $\bar{p}$. It follows that the dynamics are governed by the motion of the "slow" variables, r and c, while x and s are in quasi-steady state. Figure 6b shows the slow motion from balanced growth to the ultimate steady state. The orbit intersects the nullcline for C before intersecting the nullcline for R. It follows that c reaches a maximum before r reaches a minimum.

3. **Single-species, multiple-substrate cultures.** In this section, we consider the growth of a microbial species on mixtures of substrates. The simplest case of this formidable problem is the growth on a mixture of two growth-limiting substrates. But even binary mixtures display 4 distinct types of behavior depending on the nutrient requirements satisfied by the two substrates [6]. The two most common cases found in the modeling literature are the pairs of substitutable and complementary substrates.[5] Our extensive studies of growth on binary mixtures have been primarily concerned with mixtures of two substitutable substrates. Although we have drawn examples from the literature on mixtures of substitutable carbon sources, the phenomena described below have been observed in binary mixtures of nitrogen, phosphorus, and sulfur sources (see [21] for a comprehensive review). The theory described below therefore applies to a broad class of experiments.

To study growth on binary mixtures of substitutable substrates, we extended the model shown in Figure 1b (top) by introducing two substitutable substrates, S_1 and S_2, together with their corresponding peripheral enzymes, E_1 and E_2 (Fig. 7). This results in the equations [47, 45]

$$\dot{s_j} = D(s_j^f - s_j) - r_{s,j} c, \quad r_{s,j} \equiv V_{s,j} e_j \frac{s_j}{K_{s,j} + s_j}, \; j = 1, 2, \tag{26}$$

$$\dot{e}_j = r_{e,j}^{+} - r_{e,j}^{-} - r_g e_j, \; r_{e,j}^{+} \equiv V_{e,j} \frac{1 + K_{1,j} x_j + K_{2,j} x_j^2}{K_{3,j} + K_{1,j} x_j + K_{2,j} x_j^2}, \; r_{e,j}^{-} \equiv k_{e,j}^{-} e_j, \tag{27}$$

$$\dot{c} = (r_g - D) c, \quad r_g \equiv \sum_k Y_k r_{s,k} = \sum_k Y_k V_{s,k} e_k \frac{s_k}{K_{s,k} + s_k}, \tag{28}$$

[5]The substrates in a binary mixture are said to be complementary (or essential) if these substrates satisfy entirely distinct nutrient requirements.

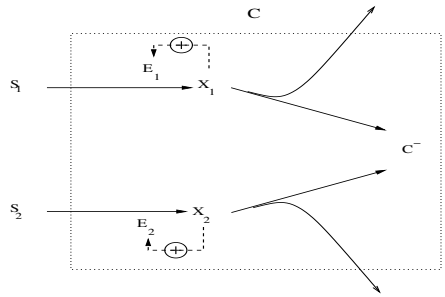

FIGURE 7. Kinetic scheme for mixed-substrate growth. Here, E_j denotes the transport enzyme catalyzing the uptake of substrate S_j, X_j denotes the inducer for E_j, and C^- denotes all intracellular components other than E_j and X_j.

where we assume that $x_j \approx r_{s,j}/k_{x,j}$, that is, the inducers rapidly attain their quasi-steady state values. We show below that this simple model successfully captures most of the observed growth patterns in both batch and continuous cultures.

3.1. **Dynamics of batch cultures.** When microbes are grown in a batch reactor containing a surplus of two substitutable substrates, one of the substrates is typically exhausted before the other, leading to the appearance of two successive exponential growth phases. During the first exponential growth phase, when both substrates are present in the medium, the cells consume either one or both the substrates. For instance, when *E. coli* K12 is grown on a mixture of fumarate and glucose, only glucose is consumed during the first phase (Figure 8a). This is called the diauxie or the preferential substrate utilization pattern, and the substrates consumed during the first and second phases are referred to as the "preferred" and "less preferred" substrates, respectively.[6] However, when *E. coli* K12 is grown on a mixture of fumarate and pyruvate, both substrates are consumed during the first phase (Fig. 8b). This is called the simultaneous substrate utilization pattern.

Studies in molecular biology have shown that the existence of different substrate utilization patterns is a manifestation of the dynamics of the peripheral enzymes for the growth-limiting substrates [7]. It is known, for instance, that the preferential substrate utilization pattern occurs because synthesis of the peripheral enzymes for the "less preferred" substrate is abolished in the presence of the "preferred" substrate. This inhibition is partly mediated by specific molecular mechanisms such as *cAMP* activation and inducer exclusion [48]. However, two lines of evidence suggest that the specific growth rates supported by the growth-limiting substrates play a crucial role. Egli notes that, in general [21],

1. The preferential substrate utilization pattern is observed whenever one of the two substrates supports a high specific growth rate. Moreover, this "rich" substrate is invariably the "preferred" substrate. However, if the initial concentration of the "preferred" substrate is decreased sufficiently, thus diminishing its ability to support growth, the two substrates are utilized simultaneously.

[6]Since glucose is consumed before fumarate, one observes two exponential growth phases separated by a stationary phase lasting a few hours. This led Monod to name the phenomenon the diauxie or "double growth."

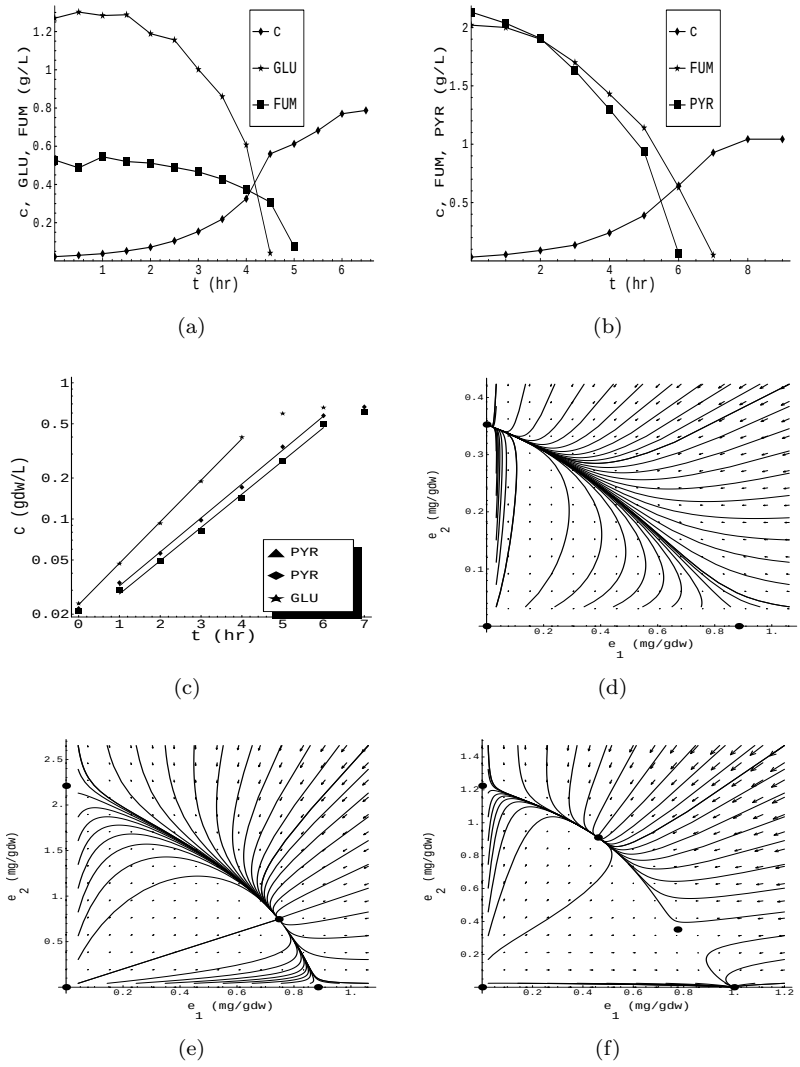

FIGURE 8. Substrate utilization patterns during batch growth on mixtures of two carbon sources. The upper panel shows the experimental data for growth of *E. coli* K12 (from [44]). (a) Sequential utilization of glucose and fumarate. (b) Simultaneous utilization of fumarate and pyruvate. (c) Initial condition dependent substrate utilization. The plots (e–f) show the global dynamics of the peripheral enzymes corresponding to these substrate utilization patterns (from [47]).

2. The simultaneous substrate utilization pattern is observed if both substrates, by themselves, support low to medium growth rates.

The model (26–28) accounts for enzyme induction and the effect of the specific growth rates (exerted through the enzyme dilution term). It ignores molecular mechanisms such as catabolite repression and inducer exclusion. However, we have

shown that although inclusion of these molecular mechanisms changes the quantitative behavior of the model, the qualitative properties remain unchanged [45, 47].

The preferential and simultaneous substrate utilization patterns are not simply determined by the nature of the two substrates in the substrate-excess batch environment. For instance, the actual substrate utilization pattern can depend on the history of the inoculum used in the experiment [11]. Figure 8c shows that if *E. coli* K12 is pregrown on glucose before exposure to a mixture of glucose and pyruvate, only glucose is consumed initially, and the specific growth rate is the same as that observed during growth on glucose alone (0.74/hr). However, if the inoculum is grown on pyruvate before exposure to a mixture of glucose and pyruvate, both substrates are consumed, and the observed specific growth rate (0.53/hr) lies between the specific growth rates on glucose (0.74/hr) and pyruvate (0.30/hr).

The foregoing substrate utilization patterns are successfully captured by the model [45, 47]. We show below that analysis of the model yields simple explanations of these seemingly complex dynamics. To this end, we note that the entire transient of batch growth is obtained by integrating differential equations (26–28) with $D = 0$. But the evolution of the peripheral enzyme levels during the *first* exponential growth phase can be described by only two equations. To see this, it suffices to observe that during the first exponential growth phase, the concentrations of both substrates are at supersaturating levels, that is, $s_j \gg K_{s,j}$ and $s_j/(K_{s,j} + s_j) \approx 1$. Under these conditions, the specific growth rate and inducer concentration(s) are approximated by the relations, $r_g \equiv \sum_k Y_k r_{s,k} \approx \sum_k Y_k V_{s,k} e_k$, $x_j = r_{s,j}/k_{x,j} \approx V_{s,j} e_j / k_{x,j}$. Moreover, constitutive enzyme synthesis is typically negligibly small ($1 \ll K_{1,j} x_j, K_{2,j} x_j^2$), and the degradation rates of the peripheral enzymes are also negligible compared to their dilution due to biomass growth $k_{e,j}^- \ll r_g$. Hence, equations (27) are closely approximated by equations

$$\begin{aligned} \dot{e}_j &= V_{e,j} \frac{\bar{K}_{1,j} e_j + \bar{K}_{2,j} e_j^2}{K_{3,j} + \bar{K}_{1,j} e_j + \bar{K}_{2,j} e_j^2} - \left(\sum_k Y_k V_{s,k} e_k\right) e_j, \\ \bar{K}_{1,j} &\equiv K_{1,j} \left(\frac{V_{s,j}}{k_{x,j}}\right), \quad \bar{K}_{2,j} \equiv K_{2,j} \left(\frac{V_{s,j}}{k_{x,j}}\right)^2. \end{aligned} \tag{29}$$

These equations, which describe the evolution of the peripheral enzyme levels during the first exponential growth phase, clearly illustrate the competition between enzymes specific to different substrates. In fact, there exists a direct analogy between the dynamics exhibited by (29) and the dynamics of the Lotka-Volterra model for competing species [42],

$$\dot{N}_j = a_j N_j - \left(\sum_k b_{jk} N_k\right) N_j, \; j = 1, 2, \tag{30}$$

where $a_j N_j$ denotes the unrestricted specific growth rate of the j^{th} species, and b_{jk} are parameters that characterize the intensity of intraspecific and interspecific competition. The only difference between (29) and (30) is the nonlinear dependence of the specific enzyme synthesis rate $r_{e,j}^+$ on e_j. Since both systems (29) and (30) are two-dimensional and strongly competitive, all of their solutions converge to some equilibria. In addition, the presence of positive inter- and intraspecific competition terms ensures that all nonnegative solutions are bounded so that both systems (29) and (30) are dissipative. Therefore, the global phase portrait in each case is

determined exclusively by the relative location and stability of equilibria.[7] In the simpler Lotka-Volterra case, at most one interior equilibrium can exist, and it is well known that

1. If a_j and b_{jk} are such that a stable interior equilibrium exists, then the global dynamics of (30) corresponds to coexistence of the species. The case where the interior equilibrium is unstable (a saddle) corresponds to bistable phase portrait of (30). The outcome of competition depends on the initial conditions.
2. If a_j and b_{jk} are such that no stable interior equilibrium exists, then the global dynamics of (30) corresponds to extinction of one of the species.

It is therefore not surprising that equations (29) can produce similar dynamics for suitable parameter values. The latter case (Fig. 8d), which shows "extinction" of E_1 during the first exponential growth phase, reflects the preferential utilization of S_2. The former case (Fig. 8e), in which both peripheral enzymes "coexist", mirrors the dynamics of simultaneous substrate utilization. The global dynamics shown in Figure 8f corresponds to preferential consumption of S_1 if the culture is pregrown on S_1 (resulting in high initial levels of E_1), and simultaneous utilization of both S_1 and S_2 if the culture is pregrown on S_2 (resulting in high initial levels of E_2). This is precisely what transpires during growth of *E. coli* on a mixture of glucose and pyruvate.

Theoretically, equations (29) may yield more complicated phase portraits due to the nonlinearity of $r^+_{e,j}$. Indeed, careful analysis of the isoclines corresponding to equations (29) shows that in addition to the competitive extinction (illustrated in Fig. 8d), coexistence (Fig. 8e), and bistability (Fig. 8e), a tri-stable phase portrait may also exist as shown in Figure 9. In the latter case, both preferred utilization patterns and the simultaneous utilization pattern may be observed with different preculture conditions.

In summary, the model suggests that the dynamics observed in mixed-substrate cultures are the outcome of "competitive interactions" between the peripheral enzymes of the substrates. Indeed,

1. Each peripheral enzyme promotes its own synthesis because production of these enzymes is autocatalytic.
2. The peripheral enzyme dynamics is competitive. Each peripheral enzyme inhibits the synthesis of the peripheral enzyme for the other substrate by increasing its intracellular dilution rate.

In terms of the model (26–28), the preferential growth pattern occurs because the "preferred" substrate increases the intracellular dilution rate of the peripheral enzyme for the "less preferred" substrate to such an extent that this enzyme becomes "extinct". The model also provides a simple explanation for the empirical generalizations stated above. Substrates that support higher growth rates tend to strongly dilute the enzymes for other substrates, and thus are likely to be the "preferred" substrates. However, in some cases, when the initial concentration of the "preferred" substrate is low in the preculture, the simultaneous substrate utilization may be observed in the experiment.

[7]The case of three and more enzymes, which we do not consider here, can be slightly more complex due to the possibility of oscillatory solutions. For instance, a complete dynamical analysis of three-dimensional Lotka-Volterra systems yields a possibility of stable positive periodic solutions [66].

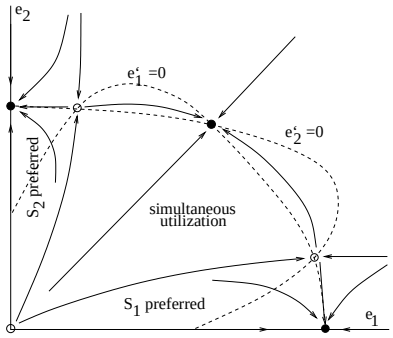

FIGURE 9. A tri-stable phase portrait of (29). The nullclines for both enzymes are shown by punctured curves. The open dots represent unstable equilibria, the filled dots represent stable equilibria. Three basins of attraction are shown for preferential utilization of S_1, simultaneous utilization of S_1 and S_2, and preferential utilization of S_2 respectively.

3.2. **Steady states of continuous cultures.** The most comprehensive study of mixed continuous cultures was reported by Egli and coworkers, who studied the growth of the methylotrophic yeasts, *H. polymorpha* and *Kloeckera* sp. 2201, on mixtures of glucose and methanol [18, 20]. In substrate-excess batch cultures, these microbes typically prefer to consume glucose before methanol. When the dilution rate was changed at fixed feed concentrations in continuous cultures, Egli et al. observed that

1. Both substrates are almost completely consumed at low dilution rates, but only glucose is consumed at high dilution rates. At such dilution rates, the residual concentration of methanol approaches its concentration in the feed which clearly indicates the lack of consumption (Fig. 10b). The dilution rate at which the pattern switches from the simultaneous to the preferential substrate utilization pattern is called the transition dilution rate.
2. The onset of the transition dilution rate is marked by a pronounced reduction in the activity of alcohol oxidase, a peripheral enzyme for methanol (Fig. 10c).
3. The transition dilution rate is higher than the washout dilution rate corresponding to single-substrate growth on methanol. In other words, consumption of methanol in the mixed-substrate culture persists at dilution rates well above the dilution rate at which the microbes are washed out of the reactor while growing on methanol alone.

Figure 10 (right panel) shows that all three phenomena can be explained within the framework of the model (26–28). We begin by explaining why the transition dilution rate exists. Before doing so, it is useful to understand the existence of the washout dilution rate since the onset of the transition dilution occurs for very similar reasons. To this end, observe that at steady state, the mass balance for the cell density yields

$$0 = (r_g - D)c \quad \Longrightarrow \quad r_g = D \ \text{ or } c = 0,$$

At low dilution rates, the steady-state satisfies the relation, $r_g = D$. As D increases, so does the specific growth rate until the cells reach the maximum specific growth rate consistent with the feed concentration. If D is increased any further, the

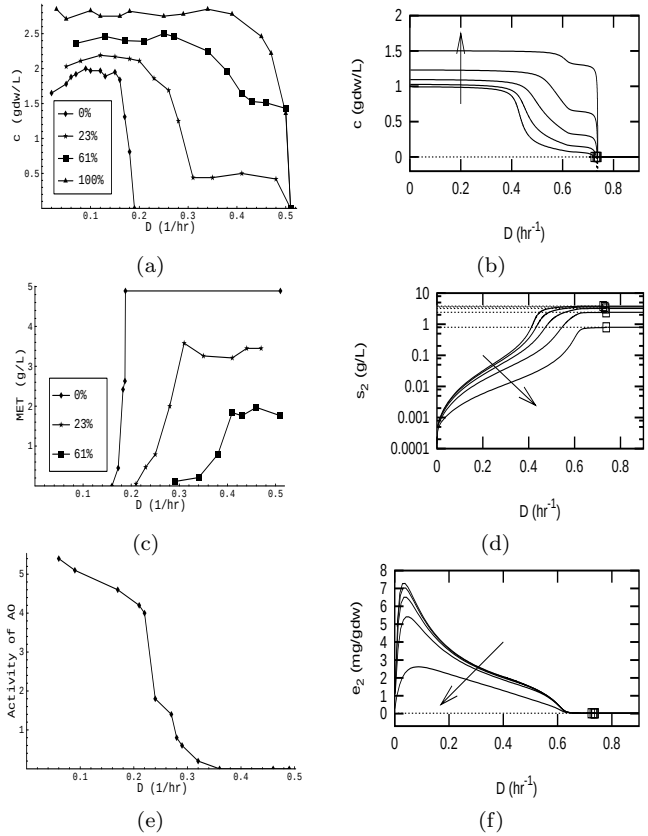

FIGURE 10. Variations of the steady-state concentrations with respect to the dilution rate at fixed feed concentrations. **Left panel:** Experimental data for growth of *H. polymorpha* on several mixtures of glucose and methanol (from [18, 20]). The total feed concentration of glucose and methanol was fixed at 5 g/L, but the proportion of glucose in the feed was varied from 0% glucose (pure methanol) to 100% glucose. (a) Cell density. (c) Methanol concentration. (e) Peripheral enzyme (alcohol oxidase) level for 61% glucose in the feed. **Right panel:** Simulations of our model (from [47]). (b) Cell density. (d) Concentration of "less preferred" substrate, S_2. (f) Peripheral enzyme level for the "less preferred" substrate. The arrows in the figures point in the direction of increasing proportion of the "preferred" substrate, S_1, in the feed.

relation $r_g = D$ can no longer be satisfied, and the cell concentration switches to the washout steady state $c = 0$ via a transcritical bifurcation. The washout dilution rate is the critical value of D that corresponds to this transcritical bifurcation. The existence of the transition dilution rate follows from a similar argument. Indeed,

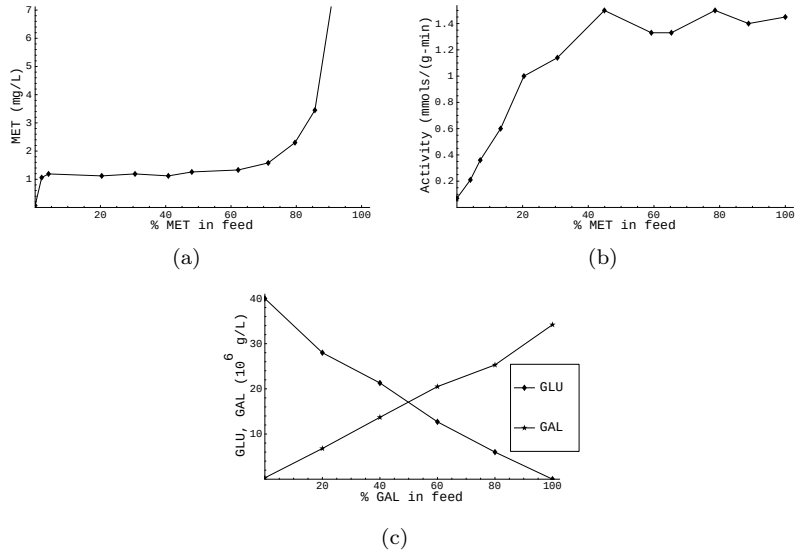

FIGURE 11. Variations of the steady-state concentrations with respect to the feed composition at a fixed dilution rate. Variation of (a) the concentration of methanol and (b) the activity of alcohol oxidase, a peripheral enzyme for methanol during growth of *Kloeckera* sp. 2201 on a mixture of glucose and methanol (from [19]). (c) Variation of the substrate concentrations during growth of *E. coli* ML308 on a mixture of glucose and galactose (from [39]).

at steady state, equation (29), the mass balance for peripheral enzymes, reads

$$V_{e,j}\frac{\bar{K}_{1,j}e_j+\bar{K}_{2,j}e_j^2}{K_{3,j}+\bar{K}_{1,j}e_j+\bar{K}_{2,j}e_j^2}=De_j \;\Rightarrow\; V_{e,j}\frac{\bar{K}_{1,j}+\bar{K}_{2,j}e_j}{K_{3,j}+\bar{K}_{1,j}e_j+\bar{K}_{2,j}e_j^2}=D \text{ or } e_j=0,$$

At sufficiently high D, the first relation cannot be satisfied, and the cells switch to a different physiological steady state with $e_j = 0$ via a transcritical bifurcation. The transition dilution rate is the value of D corresponding to such bifurcation. It is also clear that the transition dilution rate must be higher than the washout dilution rate: If the peripheral enzyme level becomes zero, then so does the corresponding substrate consumption rate, and the cells are washed out of the reactor because their specific growth rate is zero.

When the feed composition is changed at a fixed dilution rate, it is observed that (Fig. 11)

1. The peripheral enzyme levels and the residual substrate concentrations increase monotonically with the fraction of the substrate in the feed.
2. When the peripheral enzyme levels increase, the substrate concentration is constant. When the peripheral enzyme levels saturate, the substrate concentration increases.

These steady-state profiles are also predicted by the model (26–28). To understand these variations in terms of the model, we begin by observing that the steady states were obtained at dilution rates so small that nearly all of the substrate entering the chemostat is consumed ($s_j \ll s_j^f$). Under these conditions, (26) and (28) imply

that

$$c = Y_1(s_1^f - s_1) + Y_2(s_2^f - s_2) \approx Y_1 s_1^f + Y_2 s_2^f,$$

Then it follows from (26) that $r_{s,j} = D(s_j^f - s_j)/c \approx Ds_j^f/c$, and thus

$$r_{s,j} \approx \frac{Ds_j^f}{Y_1 s_1^f + Y_2 s_2^f} = \left(\frac{D}{Y_j}\right)\gamma_j, \text{ where } \gamma_j \equiv \frac{Y_j s_j^f}{Y_1 s_1^f + Y_2 s_2^f}. \tag{31}$$

Therefore, the specific substrate uptake rate of S_j is proportional to γ_j that represents the fraction of cells produced from S_j.[8] Now, since $x_j \approx r_{s,j}/k_{x,j} \approx D\gamma_j/(k_{x,j}Y_j)$, equation (27) implies that the steady-state peripheral enzyme levels are given by

$$\begin{gathered} e_j = \frac{r_{e,j}^+}{D+k_{e,j}^-} = \frac{V_{e,j}}{D+k_{e,j}^-}\frac{1+\hat{K}_{1,j}\gamma_j+\hat{K}_{2,j}\gamma_j^2}{K_{3,j}+\hat{K}_{1,j}\gamma_j+\hat{K}_{2,j}\gamma_j^2}, \\ \hat{K}_{1,j} \equiv K_{1,j}\left(\frac{D}{k_{x,j}Y_j}\right), \quad \hat{K}_{2,j} \equiv K_{2,j}\left(\frac{D}{k_{x,j}Y_j}\right)^2. \end{gathered} \tag{32}$$

Since typically $K_{3,j} \gg 1$, the steady-state peripheral enzyme levels are increasing functions of γ_j. It follows from (31) that when e_j increases linearly with γ_j, the substrate concentration is constant. When e_j saturates at large γ_j, the ratio, $s_j/(K_{s,j} + s_j)$, and hence s_j, increases with γ_j.

4. **Multiple-species, multiple-substrate cultures.** One of the most important questions in microbial ecology is that of the coexistence of mixed microbial communities supplied with mixtures of various nutritional resources. A major theoretical result based on simple phenomenological models of continuous culture is the principle of competitive exclusion stating that at most one microbial species can survive in a chemostat containing a single growth-limiting substrate [29, 30, 55, 64]. This theory extends to a very general set of functions modeling the growth response of microbes at different substrate concentrations. If the experimental growth curves for each individual species are known, the theory predicts that the species that survives at any given dilution rate and feed concentration must have the lowest break-even concentration [1, 58]. These theoretical conclusions have been confirmed by experiments [25]. To study competition for multiple substrates, a series of phenomenological models have been introduced that recognize the existence of distinct resources, and the different types of interactions between the resources [5, 10, 40, 61]. For instance, Leon and Tumpson [40] assumed that the resources are non-interacting, that is, none of the resources affect the uptake of any other resource. A model in which two substitutable resources may inhibit each others' uptake has been studied by Ballyk and Wolkowicz [5]. In their work, Ballyk and Wolkowicz presented a very detailed analysis of the model, including both local and global stability analysis. They provided important theoretical insights into the global behavior of mixed microbial cultures but formulated the results in a way that cannot be easily related to the experimental data. An important step towards reconciling theoretical predictions and experimental observations was made by Tilman,

[8] The experimental data is generally shown as a function of σ_j, the fraction of S_j in the feed. However, since γ_j is an increasing function of σ_j,

$$\gamma_j = \frac{Y_j\sigma_j}{Y_1\sigma_1 + Y_2\sigma_2}, \ \sigma_j \equiv \frac{s_j^f}{s_1^f + s_2^f},$$

the general trends (increasing or decreasing) are the same regardless of the parameter used to plot the data.

who developed an elegant graphical theory of two-species growth on arbitrary mixtures of substrates [61, 62]. Specifically, Tilman demonstrated that the existence and stability of coexistence equilibria corresponding to a given combination of the feed concentrations and the dilution rate can be deduced from single-species data. In light of the above theoretical findings and given our goal of developing a unifying physiological theory of microbial growth, we were naturally led to ask the questions,

> *Given the experimental data on the mixed-substrate growth of individual species, can we predict the outcome of an experiment in which all these species are inoculated in the chemostat? How do these predictions relate to the underlying physiological principles governing microbial growth?*

As a starting point, we considered the growth of two species on a mixture of two substitutable substrates. In [52, 53], we showed that if the interaction between the two species is purely competitive, all the key properties of the mixed-culture steady states can indeed be predicted from the single-species data.

The foregoing question was motivated by the desire to predict mixed-culture growth from the experimental data for single-species growth on mixtures of substrates. However, as shown above, the single-species model (26–28) successfully captures the experimental data. Thus, it seems pertinent to ask whether the model itself can be used to study mixed-culture behavior. To this end, we studied the competition between two species, each of which consumes the same pair of substitutable substrates in accordance with the kinetic scheme shown in Figure 7. We asked the question,

> *Under what operating conditions can two species coexist in a chemostat limited by two substrates?*

In [56], we constructed an operating diagram that shows all the dilution rates and feed concentrations at which two species can coexist.

4.1. **Deducing mixed-culture dynamics from single-species data.** To demonstrate that mixed-culture growth can be predicted from single-species data, we began by considering a simple phenomenological model of mixed growth [52].

The phenomenological model has the form

$$\dot{s}_j = D(s_j^f - s_j) - c_1 r_{1j}^s(s_1, s_2) - c_2 r_{2j}^s(s_1, s_2), \quad j = 1, 2, \tag{33}$$

$$\dot{c}_i = c_i\Big(r_i^g(s_1, s_2) - D\Big), \quad i = 1, 2, \tag{34}$$

where r_i^g denotes the specific growth rate of the i^{th} species and r_{ij}^s denotes the specific substrate uptake of the j^{th} substrate by the i^{th} species. We assumed that the two substrates are substitutable, so that $r_i^g(s_1, s_2) = Y_{i1} r_{i1}^s(s_1, s_2) + Y_{i2} r_{i2}^s(s_1, s_2)$. Here, the coefficients $Y_{ij},\ i, j = 1, 2$ denote the growth yields of the i^{th} species on the j^{th} substrate respectively, and we assume that all these yields are constant. In addition, we assume that each substrate stimulates its own uptake

$$\frac{\partial r_{i1}^s}{\partial s_1}(s_1, s_2) \geq 0, \quad \frac{\partial r_{i2}^s}{\partial s_2}(s_1, s_2) \geq 0, \tag{35}$$

but inhibits the uptake of the other substrate

$$\frac{\partial r_{i1}^s}{\partial s_2}(s_1, s_2) \leq 0, \quad \frac{\partial r_{i2}^s}{\partial s_1}(s_1, s_2) \leq 0. \tag{36}$$

This property of mutual inhibiton was inherent in the physiological model (26–28) for two substitutable substrates: Substrate S_i inhibited the uptake of substrate

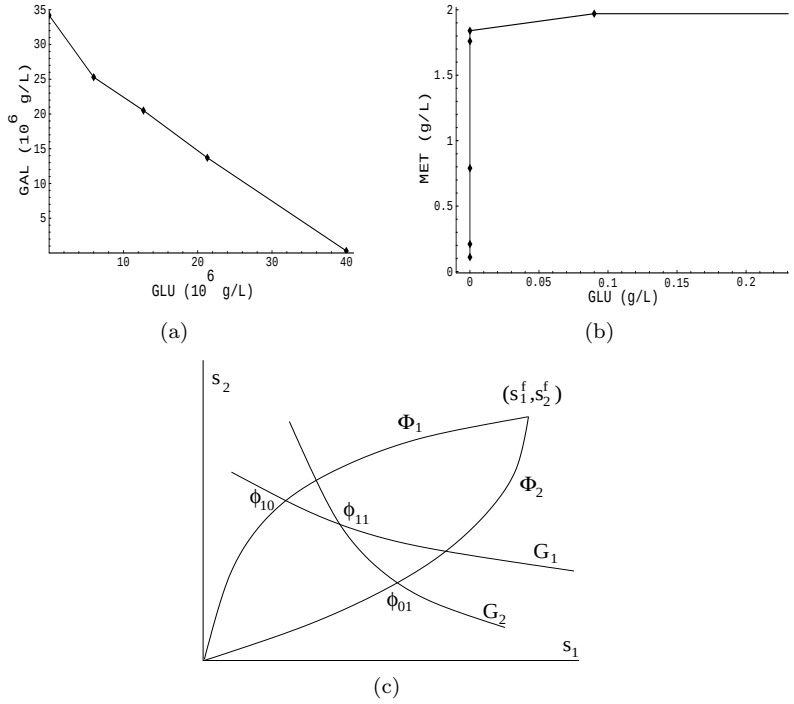

FIGURE 12. (a) The growth isocline for *E. coli* ML308 growing on a mixture of glucose and galactose at $D = 0.3$ 1/hr. The curve was derived from the data shown in Figure 11c. (b) The consumption curve for *H. polymorpha* growing on a mixture of 61% glucose and 39% methanol. The curve was derived from the data shown in Figure 10b. (c) Determination of the existence, uniqueness, and stability of the steady-states from the growth isoclines and consumption curves for the two species. The growth isoclines for species 1 and 2 are labeled G_1 and G_2, respectively. The consumption curves for species 1 and 2 are labeled Φ_1 and Φ_2, respectively. The semitrivial steady-state, $c_1 > 0, c_2 = 0$ is denoted by the point ϕ_{10}; the semitrivial steady-state, $c_2 > 0, c_1 = 0$ is denoted by the point ϕ_{01}; and the nontrivial (coexistence) steady-state, $c_1 > 0, c_2 > 0$ is denoted by the point ϕ_{11}. Coexistence is stable for the disposition of the curves shown in the figure.

$S_j, j \neq i$ by enhancing the intracellular dilution rate of E_j. In the phenomenological model (33 –34), we simply assume the mutual inhibition property without prescribing a mechanism for it.[9]

The phenomenological model (33–34) admits three types of steady states: Trivial ($c_1 = c_2 = 0$), semitrivial ($c_1 > 0, c_2 = 0$ and $c_1 = 0, c_2 > 0$), and nontrivial ($c_1, c_2 > 0$). Our main result was that the existence, uniqueness, and stability of

[9]Although equations (33–34) are algebraically identical to the model studied by Ballyk and Wolkowicz [5], we analyzed the model under a less restrictive set of assumptions and used a different analytic approach.

these steady-states can be inferred from two curves, that are completely determined by the experimentally observed steady-states of single-species growth on S_1 and S_2. These curves are defined as follows

1. The growth isocline of the i^{th} species, denoted G_i, is the locus of all steady-state substrate concentrations, (s_1, s_2), obtained when this species alone is grown on a mixture of S_1 and S_2 at a *fixed dilution rate*, but varying feed concentrations (Fig. 12a). For the phenomenological model, G_i is given by the relation
$$r_i^g(s_1, s_2) = D, \tag{37}$$
which follows from (34).
2. The consumption curve of the i^{th} species, denoted Φ_i, is the locus of all steady state substrate concentrations, (s_1, s_2), obtained when this species alone is grown on a mixture of S_1 and S_2 at fixed feed concentrations, but varying dilution rates (Fig. 12b). For the unstructured model, Φ_i is given by the relation
$$\frac{s_1^f - s_1}{r_{i1}^s(s_1, s_2)} = \frac{s_2^f - s_2}{r_{i2}^s(s_1, s_2)} \geq 0, \tag{38}$$
which follows from (33) with $c_j = 0, j \neq i$. Given the assumptions (35–36) regarding the specific substrate uptake rates, it can be shown that the consumption curve is a monotonically increasing function passing through the points, $(0, 0)$ and (s_1^f, s_2^f).

Using the definitions of these curves, it is easy to see that

1. The projection of any semitrivial steady-state ($c_i > 0, c_j = 0, j \neq i$) onto the (s_1, s_2) plane lies at the intersection of the corresponding growth isocline, G_i, and the consumption curve, Φ_i.
2. The nontrivial (coexistence) steady state(s), $c_1, c_2 > 0$, exist if and only if the two growth isoclines intersect within the envelope of coexistence, defined as the region in the (s_1, s_2) plane enclosed by the two consumption curves. If an (s_1, s_2)-projection of a nontrivial steady-state falls outside of the envelope of coexistence, at least one of the resulting two cell densities is negative.
3. The dynamics of both single-species cultures are completely determined by the intersections of the corresponding growth isocline and the consumption curve. Indeed, suppose for a moment that $c_2 \equiv 0$. Then the model (33–34) reduces to three equations
$$\begin{aligned} \dot{s}_1 &= D(s_1^f - s_1) - c_1 r_{11}^s(s_1, s_2), \\ \dot{s}_2 &= D(s_2^f - s_2) - c_1 r_{12}^s(s_1, s_2), \\ \dot{c}_1 &= c_1\Big(Y_{11} r_{11}^s(s_1, s_2) + Y_{12} r_{12}^s(s_1, s_2) - D\Big). \end{aligned}$$
Letting $z = Y_{11}s_1 + Y_{12}s_2 + c_1$, we find that $\dot{z} = D(Y_{11}s_1^f + Y_{12}s_2^f - z)$, thus the above equations enjoy the asymptotic consevration law $z = Y_{11}s_1^f + Y_{12}s_2^f$. Hence, the above system can be effectively reduced to two equations
$$\dot{s}_1 = D(s_1^f - s_1) - \Big\{Y_{11}(s_1^f - s_1) + Y_{12}(s_2^f - s_2)\Big\} r_{11}^s(s_1, s_2), \tag{39}$$
$$\dot{s}_2 = D(s_2^f - s_2) - \Big\{Y_{11}(s_1^f - s_1) + Y_{12}(s_2^f - s_2)\Big\} r_{12}^s(s_1, s_2). \tag{40}$$
It is easy to see that the system (39–40) is strictly cooperative for $0 < s_j \leq s_j^f$. Therefore, all positive solutions converge to some equilibria whose stability

is determined by the intersections of G_1 and Φ_1. Imortantly, a single-species culture cannot exhibit any type of oscillatory behavior.[10]

The existence and uniqueness of the mixed-culture steady states is also completely determined by the growth isoclines and consumption curves for the two species. It is interesting that the stability of the steady states is also determined by these curves. To this end, it is useful to classify the interaction between the substrates for a given species. Specifically, the substrates are said to be locally synergistic (resp. locally antagonistic) for the i^{th} species if increasing both substrate levels along the consumption curve Φ_i increases (resp. decreases) the specific growth rate r_i^g. Stability analysis of the equations (33–34) shows that

1. The semitrivial steady states are stable if and only if the substrates are locally synergistic and the other competitor cannot invade the chemostat.
2. The nontrivial steady states are stable only if the following inequality is satisfied at the steady state
$$\left[-\frac{\partial r_1^g/\partial s_2}{\partial r_1^g/\partial s_1}-\left(-\frac{\partial r_2^g/\partial s_2}{\partial r_2^g/\partial s_1}\right)\right]\cdot\left[\frac{r_{11}^s}{r_{12}^s}-\frac{r_{21}^s}{r_{22}^s}\right]>0. \tag{41}$$
The first term is the difference between the slopes of the two growth isoclines at the nontrivial steady state. The second term is positive if and only if Φ_1 lies above Φ_2. If the latter is true, (41) says that coexistence is stable only if the difference between the slopes of the growth isoclines is positive (Fig. 12).

It turns out that inequality (41) is necessary but not sufficient for the stability of a nontrivial equilibrium. In [52], we have demonstrated that Hopf bifurcations may occur in the region where (41) holds, provided that the substrates S_1 and S_2 are locally synergistic for one species and locally antagonistic for the other.

The foregoing results concerning the existence, uniqueness, and stability of the steady states are preserved even if additional physiological structure is added to the model. In [53], we extended the phenomenological model (33–34) by explicitly considering the physiological structure for each of the microbial species as shown in Figure 7. The equations of this physiological model are

$$\dot{s}_j = D(s_j^f - s_j) - c_1 r_{1j}^s - c_2 r_{2j}^s,\ j=1,2, \tag{42}$$
$$\dot{e}_{ij} = r_{ij}^e(s_j, e_{ij}) - e_{ij} r_i^g(s_1, s_2, e_{i1}, e_{i2}), \tag{43}$$
$$\dot{c}_i = \left(r_i^g(s_1, s_2, e_{i1}, e_{i2}) - D\right) c_i,\ i=1,2, \tag{44}$$

where $r_i^g \equiv Y_{i1} r_{i1}^s + Y_{i2} r_{i2}^s = Y_{i1} e_{i1} \sigma_{i1} + Y_{i2} e_{i2} \sigma_{i2},\ i=1,2$. In [53], we presented the local stability analysis of (42–44) based on the following assumptions,

(H1): The functions $r_{ij}^e(s_j, e_{ij})$ are such that
$$\frac{\partial r_{ij}^e(s_j,e_{ij})}{\partial s_j}>0, \quad \frac{\partial}{\partial e_{ij}}\left(\frac{r_{ij}^e(s_j,e_{ij})}{e_{ij}}\right)<0.$$
For any $s_j > 0$,
$$\lim_{e_{ij}\to 0} r_{ij}^e(s_j, e_{ij}) = e_{ij}^*(s_j) > 0,$$
and there exists a unique value $e_{ij}^0(s_j) > 0$ such that $r_{ij}^e(s_j, e_{ij}^0(s_j)) = 0$.

(H2): The functions r_{ij}^s are given by $e_{ij}\sigma_{ij}(s_j)$, where $\sigma_{ij}(s)$ are such that
$$\sigma_{ij}(0)=0,\ \sigma_{ij}'(s)>0,\ \lim_{s\to\infty}\sigma_{ij}(s)<+\infty.$$

[10]This proof was originally presented in [5] for the case when the semitrivial steady-state is unique.

Using hypotheses (H1) and (H2), we obtained the following results

1. Under steady-state growth conditions, the substrate concentrations uniquely determine the physiological state of the cell, including the mass fractions of the peripheral (transport) enzymes and the inducer molecules. Specifically, we showed that for all combinations (s_1, s_2) of the substrate concentrations, the peripheral enzyme levels e_{ij} exhibit a unique positive steady state. Denoting this physiological steady state by $e_{ij} = e_{ij}(s_1, s_2)$, we redefined the notions of the growth isocline and the consumption curve. For instance, the growth isocline G_i for the i^{th} species is the locus of all substrate concentrations such that
$$Y_{i1}e_{i1}(s_1, s_2)\sigma_1(s_1) + Y_{i2}e_{i2}(s_1, s_2)\sigma_2(s_2) = D.$$
2. The growth isocline, G_i, is a graph of a decreasing function in the (s_1, s_2) plane, while the consumption curve Φ_i is a graph of an increasing function in the (s_1, s_2) plane connecting the origin to the point (s_1^f, s_2^f).
3. There exists at most one semitrivial steady state for a given i, and it lies at the intersection of the corresponding growth isocline and the consumption curve. The stability of the semitrivial steady state is determined by the ability of the resident species to defend the chemostat against occupation by the other species.
4. The nontrivial (coexistence) steady-state is represented by an intersection of two growth isoclines if and only if it occurs within the envelope of coexistence, that is, the region between the two consumption curves. We also showed that the necessary condition for the stability of the nontrivial equilibrium of (42–44) is identical to (41). Finally, we demonstrated that model (42–44) may admit multiple nontrivial equilibria.

These conclusions were heavily based on hypothesis (H1) which essentially warranted the uniqueness of the physiological steady-state. If the assumption (H1) is not valid, for instance, when one of the functions $\frac{r_{ij}^e(s_j, e_{ij})}{e_{ij}}$ is no longer monotonically decreasing in the corresponding e_{ij}, then multiple physiological steady states may exist. We have already discussed this possibility in section 3.1. This case requires an extensive additional analysis which we are currently conducting.

4.2. **The operating diagram for coexistence of species.** In [56], we determined the operating diagram of the model (42–44), and presented a computational procedure that allows to explicitly compute the dilution rates and feed concentrations at which two species, C_1 and C_2, coexist in the chemostat supplied with two substitutable substrates S_1 and S_2. At a coexistence steady-state, the algebraic system
$$\begin{aligned} r_{11}^s c_1 + r_{21}^s c_2 &= D(s_1^f - s_1), \\ r_{12}^s c_1 + r_{22}^s c_2 &= D(s_2^f - s_2), \end{aligned}$$
must admit a positive solution (c_1, c_2). Moreover, the residual substrate concentrations are negligibly small compared to the feed concentrations ($s_j \ll s_j^f$) at all but the highest dilution rates and/or the smallest feed concentrations. Under these conditions, the coexistence steady-state satisfies the vectorial relation
$$c_1\mathbf{r}_1^s + c_2\mathbf{r}_2^s = D\mathbf{s}^f, \text{ where } \mathbf{r}_i^s = (r_{i1}^s, r_{i2}^s)^T, \ \mathbf{s}^f = (s_1^f, s_2^f)^T,$$
with $c_i > 0$. Hence, the vector $\mathbf{s}^f$ must lie in the positive cone spanned by the vectors $\mathbf{r}_1^s$ and $\mathbf{r}_2^s$. In [56], we chose the parameter values such that C_1 prefers S_1,

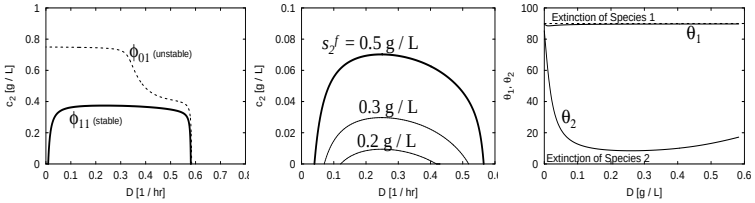

(a) (b) (c)

FIGURE 13. (a) Species 2 vanishes at sufficiently small dilution rates. (b) The smaller the feed concentration, s_2^f, the smaller the interval of coexistence. (c) Operating diagram showing the feed concentration ratios at which the two species can coexist. At any given dilution rate, species 1 cannot exist, if s_2^f is so high compared to s_1^f that $\arctan(s_2^f/s_1^f)$ lies above the curve θ_1. Likewise, species 2 cannot exist, if s_2^f is so low compared to s_1^f that $\arctan(s_2^f/s_1^f)$ lies below the curve θ_2. Coexistence is feasible only if s_2^f/s_1^f is such that $\arctan(s_2^f/s_1^f)$ lies between the curves θ_1 and θ_2.

and C_2 prefers S_2 (e.g. $r_{11}^s > r_{21}^s$, and $r_{12}^s < r_{22}^s$). Then we suggested a concise way of depicting the operating diagram: Let $\theta_i(D)$ and θ_s denote the angles formed by $\mathbf{r}_i^s$ and $\mathbf{s}^f$ with the s_1^f-axis. It is easy to see that the above choice of substrate preference corresponds to the inequality $\theta_1(D) < \theta_2(D)$. Therefore, the operating diagram can be represented by a region in the (D, θ)-plane defined by the inequality $\theta_1(D) < \theta_s < \theta_2(D)$.

The simulations showed that when both species are grown in the reactor, C_2 vanishes at a sufficiently low dilution rate. Thus, both species coexist only if the dilution rate lies within a certain interval (Fig. 13a). The smaller the feed concentration of S_2, the preferred substrate for C_2, the smaller the width of the interval. At sufficiently small s_2^f, the width of the interval vanishes, so that C_2 cannot exist at any dilution rate (Figure 13b). Similar behavior is observed if the feed concentration of S_1 is decreased. At sufficiently small s_1^f, C_1 cannot exist at any dilution rate. Thus, the operating diagram has the form shown in Figure 13c. If $s_1^f \gg s_2^f$, species 2 cannot exist at any dilution rate; likewise, if $s_1^f \ll s_2^f$, species 1 cannot exist at any dilution rate. Coexistence is feasible for some range of dilution rates only if the ratio of the feed concentration lies within a certain range.

5. **Discussion.** Although the above models provide a useful starting point, much remains to be done. In this section, we describe some of the outstanding problems that must be resolved to develop a truly comprehensive physiological theory of microbial growth.

5.1. **Single-species, single-substrate cultures.**

5.1.1. *The role of energy.* Figure 1a shows that the precursor pool, P, has several possible fates - RNA/protein synthesis, respiration, storage and excretion. The question then arises

What determines the relative rates of RNA/protein synthesis, respiration, storage, and excretion?

This question is important in its own right. Moreover, as we show below, the characteristics of mixed-substrate growth rest crucially upon a proper understanding of this question.

The experimental evidence suggests that microbial cells control and regulate these metabolic processes in a seemingly rational manner. Under starvation conditions, cells increase the respiration rate relative to the growth rate. Under carbon-excess conditions, they synthesize carbohydrates at the expense of RNA and proteins. It is believed that nucleotide phosphates such as ATP and ADP, the "energy currency" of the cell, play a supervisory role in organizing these reactions. The nucleotide phosphates are global variables, inasmuch as they are involved in virtually all the intracellular reactions. To study the role of energy conversions in organizing cell growth, one could modify the kinetic scheme shown in Figure 1a by coupling all the processes to ATP synthesis or consumption. For instance, peripheral catabolism of the substrate, and synthesis of RNA, proteins, and carbohydrates are energy-consuming processes coupled to the conversion of ATP to ADP. On the other hand, respiration, excretion, and the generation of P from X and P_s are energy-releasing processes coupled to the conversion of ADP to ATP. Since ATP is a "fast" variable, the rate of energy synthesis and consumption are approximately equal on the time scale of interest. This "energy balance" imposes a constraint on the relative rates of the key processes. It is conceivable that additional constraints, such as "redox balances", may be necessary to obtain full agreement with the data. Such an extended model could yield the relative rates of biosynthesis, respiration, storage, and excretion.

5.2. **Single-species, multiple-substrate cultures.** We have shown above that a simple model of growth on mixtures of substitutable substrates captures the dynamics of batch cultures and the steady states of continuous cultures. However, there are open questions regarding the dynamics of continuous cultures. Insofar as mixtures of complementary substrates are concerned, there are hardly any physiological models.

5.2.1. *Mixtures of substitutable substrates.* Two types of experiments have been performed to study the dynamics of mixed-substrate growth in a chemostat. We show below that the first type of transient can be understood in terms of our existing model, but the second reveals a deficiency of the model.

We begin by describing the transients that fall within the scope of our existing model. Harte and Webb studied the response of glucose-limited cells of *K. aerogenes* to substrate switches [3, 27]. The cells were allowed to reach steady state in a chemostat at a feed concentration of 100 mg/L. After steady state was reached, the feed was changed to a mixture of glucose (100 mg/L) and maltose (100 mg/L). Since the feed concentration was increased, the cell density is expected to increase. However, it turns out that the rate of increase depends on the dilution rate at which the experiment is performed (Fig. 14a). At low dilution rates, uptake of maltose commences immediately after the shift, and the cell density increases without any lag. At intermediate dilution rates, there is a lag before maltose uptake and growth. At high dilution rates, there is neither maltose uptake nor growth. This data can be understood in terms of our existing model. During steady-state growth on glucose, the concentration of the inducer for maltose is zero. Hence, (27) implies

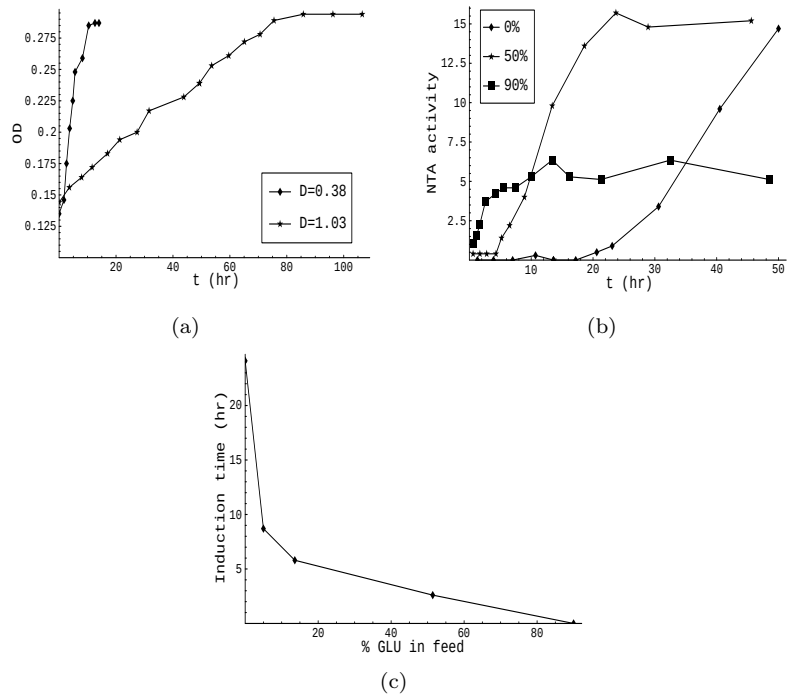

FIGURE 14. Dynamics of growth on mixtures of substitutable substrates. (a) Transient response of glucose-limited cultures of *K. aerogenes* to feed switches from glucose (100 mg/L) to glucose (100 mg/L) plus maltose (100 mg/L). The data shows that the larger the dilution rate at which the feed is switched, the longer the lag before the OD increases. (b) Induction of NTA metabolism in *C. heintzii* growing in continuous culture after switching the feed from a medium containing glucose as the sole carbon source to a medium containing glucose and NTA. The data shows that the higher the percentage of glucose in the feed, the smaller the time required to induce NTA metabolism. (c) Induction times corresponding to various proportions of glucose in the feed.

that immediately after the substrate switch, the activity of the peripheral enzyme for maltose is

$$e_{\mathrm{MAL}} = \frac{V_{e,\mathrm{MAL}}}{K_{3,\mathrm{MAL}}\left(D + k^{-}_{e,\mathrm{MAL}}\right)}.$$

According to this expression, the higher the dilution rate, the smaller the activity of the peripheral enzymes for maltose. It follows that the higher the dilution rate at which the feed is switched from pure glucose to a mixture of glucose and maltose, the longer it takes to accumulate the peripheral enzymes for maltose. At dilution rates exceeding the transition dilution rate for maltose, the peripheral enzyme levels are so small that there is no observable uptake of maltose.

Bally and Egli [4] studied another type of substrate switch resulting in dynamics that are beyond the scope of our current model. They allowed glucose-limited cells

of *C. heintzii* to reach steady state, after which the feed was abruptly switched to a mixture of glucose and nitrotriacetic acid (NTA). Since the cells have not seen NTA until after the switch, one expects a lag before the peripheral enzymes for NTA are induced. Furthermore, intuition suggests that the larger the concentration of glucose in the feed, the larger the induction time. The experiments show precisely the opposite result (Fig. 14b). When the feed is switched to pure NTA, the induction time is 20 hours. When the feed is switched to 50% glucose and 50% NTA, the induction time drops dramatically to 4 hours, and with 90% glucose, there is no induction lag at all. This data shows that under these conditions, glucose supports, rather than inhibits, the induction of the peripheral enzymes for NTA. To understand this counterintuitive result, recall that when the feed is switched from pure glucose to pure NTA, the uptake of NTA is negligibly small (see Fig. 2), so that the cells are presumably in a "starvation" state. However, when the feed is switched from pure glucose to a mixture of glucose and NTA, uptake of NTA is vanishingly small, but glucose is consumed significantly. It is conceivable that the energy and precursors derived from catabolism of glucose mitigate the starvation state, and either stimulate the synthesis, or inhibit the degradation, of the peripheral enzymes for NTA. It turns out that this is indeed the case. Bally and Egli showed that if the feed is switched from NTA to a medium containing no carbon source, thus depriving the cells of energy and precursors, the degradation rate of the peripheral enzymes for NTA is 0.3-0.9 1/hr. However, when the feed is switched from pure NTA to pure glucose, the degradation rate of the peripheral enzymes for NTA is only 5% per hour. The foregoing results cannot be reconciled with our current model since it does not even consider the energy levels as variables. To capture these results, it is necessary to incorporate the energy levels in the manner described above. The degradation rates of the enzymes can then be defined in terms of the energy status of the cells. These modifications could lead to agreement with the data.

5.2.2. *Mixtures of complementary substrates.* In most experiments with complementary mixtures, the growth-limiting substrates are the carbon and nitrogen sources. It is intuitively obvious that a culture is carbon limited if the carbon-to-nitrogen (C:N) ratio in the medium is small, and nitrogen limited if the C:N ratio is large. The central question that then arises is

> *What physiological changes do the cells undergo as the medium is changed from carbon- to nitrogen-limited conditions and* vice versa*?*

In the modeling literature, growth on complementary substrates is commonly described by phenomenological models that assume the mixed-substrate specific growth rate of the form

$$r^g(s_1, s_2) = \min\left\{r_1^g(s_1),\, r_2^g(s_2)\right\},$$

where $r_i^g(s_j)$ are increasing functions of s_j describing the specific growth rate under S_j-limited conditions [40, 61, 31]. These phenomenological models have been subsequently generalized using the cell-quota formulation originally due to Droop [14, 15] partially decoupling the processes of substrate uptake and growth [34, 38, 13]. All of the above models have the property that at steady state the cells are either carbon limited or nitrogen limited unless $r_1^g(s_1) = r_2^g(s_2)$. This curve describes a sharp interface between the regimes of different substrate limitations. As we show below, this contradicts the experimental data.

Durner and Egli determined the steady-states in a chemostat when the feed concentration of the nitrogen source (ammonia) and the dilution rate are held fixed,

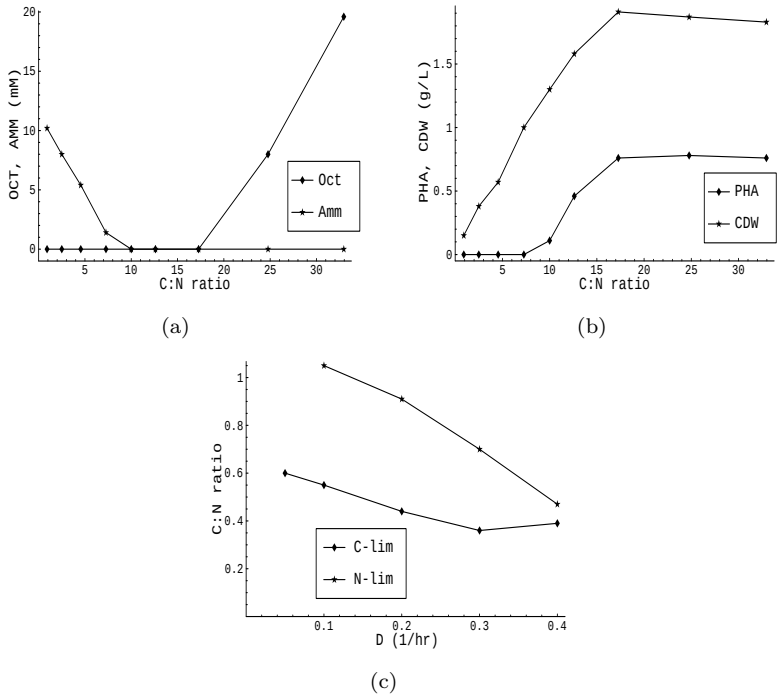

FIGURE 15. Variations of the steady-state concentration during growth of *P. oleovarans* on a medium containing octanoate and ammonia as the sole carbon and nitrogen sources (from [16, 17]). The dilution rate was fixed at 0.2 1/hr, and the carbon:nitrogen (C:N) ratio in the feed was varied. (a) The concentration of octanoate (resp. ammonia-N) is an increasing (resp. decreasing) function of the C:N ratio. However, there is an intermediate range of C:N ratios ($10 \leq$ C:N ≤ 17) at which both octanoate and ammonia are almost completely consumed. This is the so-called dual-substrate-limited regime. (b) In the dual-substrate-limited regime, the increase in dry cell weight is entirely due to accumulation of polyhydroxyalkanoates (PHA). (c) The negative correlation between the dilution rate and the range of C:N ratios at which the culture is dual substrate limited.

but the feed concentration of the carbon source (octanoate) is progressively increased [16, 17]. Figure 15a shows that as expected, growth is carbon limited (the residual concentration of the carbon source is negligibly small) when the C:N ratio of the feed is small, and nitrogen limited when the C:N ratio of the feed is large. It is clear, however, that the transition from carbon to nitrogen limitation is not sharp. There is a wide range of C:N ratios at which the cells are both carbon *and* nitrogen limited. This transition zone is called the dual-substrate-limited regime.

The existence of the dual-substrate-limited regime is intimately connected with the cell's ability to store nutrients. At the lower boundary of the dual-substrate-limited regime, the residual concentration of the nitrogen source is vanishingly small (Fig. 15a). Hence, further provision of carbon by increasing the C:N ratio of the feed

cannot support additional RNA and protein synthesis. Yet Figure 15a shows that the cells still consume the additional carbon since the residual concentration of the carbon source remains negligibly small. Moreover, the additional carbon consumed must result in the synthesis of some component of biomass because the cell density continues to increase (Fig. 15b). It turns out that the additional carbon consumed is completely channeled into the storage component, polyhydroxyalkanoates (PHA). Synthesis of PHA persists until the cell's capacity for storing PHA is saturated, at which point cells are unable to consume additional carbon in the feed, and it simply passes through the reactor. Thus, storage provides a kind of "buffer" that smoothes the transition from carbon to nitrogen limited growth.

Interestingly, the width of the dual-substrate-limited regime depends on the dilution rate at which the experiment is performed. The larger the dilution rate, the smaller the width of the transition zone (Fig. 15c). As the dilution rate approaches the maximum specific growth rate, the width becomes zero.

The behavior can be captured by a slight modification of the kinetic scheme shown in Figure 1a. It turns out the ammonia is required for synthesis of amino acids (M), which in turn are required for synthesis of proteins (C^-) and RNA (R). Now, under nitrogen-limiting conditions, the exogenous ammonia levels are low, the synthesis rates of amino acid, proteins, and RNA synthesis are necessarily small. Since the exogenous carbon is in excess, the cells respond by channeling the excess carbon into carbohydrate (P_s). Now, the primary goal of a model is to predict Figure 15c, that is, the operating diagram that describes the regime of dual substrate limitation in terms of the dilution rate and feed concentrations. It seems to us that the achievement of this goal hinges upon the ability to predict the relative rates of storage and RNA/protein synthesis. As mentioned above, energetics certainly plays a critical role in determining the relative rates of these processes under carbon-limited conditions. The crux of the problem here is to ascertain whether the energetic constraints also determine the relative rates of these processes under nitrogen and dual-substrate-limited conditions.

5.3. **Multiple species, multiple-substrate cultures.** In [52, 53], we studied models of pure competition. The pure competition models assume that different microbial species interact only by consuming and utilizing the substrates thus making these substrates unavailable to other competitors. In reality, interactions between distinct species can be more complicated. A particularly interesting type of interaction is *commensalism* in which one of the competing species excretes a metabolite that supports the growth of the other species. It is also conceivable that the interaction is amensalistic - one species excretes a toxic product that inhibits the growth of the other species.

The effects of such nonpure competition on the dynamics of mixed cultures can be studied by modifying equations (42–44). For example, suppose that in the model (42–44), species C_1 excretes a product S_3 that supports the growth of species C_2. We can include this new feature in the model by considering two additional mass balance equations for S_3 and the corresponding peripheral enzyme E_{23} of the form

$$\dot{s}_3 = \varepsilon r_1^g c_1 - D s_3 - r_{23}^s c_2, \quad r_{23}^s = e_{23}\sigma_{23}, \tag{45}$$

$$\dot{e}_{23} = R_{23}(s_1, s_2, s_3, e_{21}, e_{22}, e_{23}), \tag{46}$$

and change the specific growth rate r_2^g to

$$r_2^g = Y_{21} r_{21}^s + Y_{22} r_{22}^s + Y_{23} r_{23}^s,$$

where the last term represents the increment in the specific growth of species 2 due to consumption of S_3. In [56], we studied this modification of the model numerically, but it lends itself equally well to analytical methods. Observe that if $\varepsilon = 0$, the new model has the same behavior as (42–44), which we have already studied in considerable detail. The new model with small $\varepsilon > 0$ could be analyzed by using local perturbation techniques, and then appealing to continuation arguments to extend the analysis to a broader parameter region.

Acknowledgment. The authors are grateful to Profs. Yang Kuang and Hal Smith for their valuable comments. A part of this work was completed while S. S. P. was visiting the Mathematical Biosciences Institute at The Ohio State University.

Appendix A. **Derivation of the reduced equations (19–25).** Defining the dimensionless variables in (12–18) as

$$\hat{s} \equiv \frac{s}{s_r}\,,\ \hat{c} \equiv \frac{c}{s_r}\,,\ \hat{x} \equiv \frac{x}{x_r}\,,\ \hat{e} \equiv \frac{e}{e_r}\,,\ \hat{r} \equiv \frac{r}{r_r}\,,\ \hat{p} \equiv \frac{p}{p_r}\,,\hat{c}^- \equiv \frac{c^-}{c_r^-}\ \hat{t} \equiv \frac{t}{t_r},$$

where

$$\begin{array}{cccc} s_r = s_f, & c_r = s_f, & x_r = \sqrt{\frac{V_s V_e}{k_x}}, & e_r = \sqrt{\frac{V_e}{V_s}}, \\ r_r = \frac{\sqrt{V_s V_e}}{V_c}, & p_r = \frac{\sqrt{V_s V_e}}{k_{\mathrm{co}_2}}, & c_r^- = 1, & t_r = \frac{1}{\sqrt{V_s V_e}}, \end{array}$$

we obtain the dimensionless equations,

$$\frac{d\hat{s}}{d\hat{t}} = \hat{D}(1-\hat{s}) - \hat{r}_s\hat{c}, \tag{47}$$

$$\frac{d\hat{c}}{d\hat{t}} = \left(\hat{r}_g - \hat{D}\right)\hat{c}, \tag{48}$$

$$\frac{d\hat{e}}{d\hat{t}} = \hat{r}_e^+ - \hat{r}_e^- - \hat{r}_g\hat{e}, \tag{49}$$

$$\frac{d\hat{r}}{d\hat{t}} = \hat{r}_r^+ - \hat{r}_r^- - \hat{r}_g\hat{r}, \tag{50}$$

$$\tau_x\frac{d\hat{x}}{d\hat{t}} = \hat{r}_s - \hat{r}_x - \tau_x\hat{r}_g\hat{x}, \tag{51}$$

$$\tau_p\frac{d\hat{p}}{d\hat{t}} = \hat{r}_x - \hat{r}_{\mathrm{co}_2} - \left(\hat{r}_c^+ - \hat{r}_c^-\right) - r_r\left(\hat{r}_r^+ - \hat{r}_r^-\right) - e_r\left(\hat{r}_e^+ - \hat{r}_e^-\right) - \tau_p\hat{r}_g\hat{p}, \tag{52}$$

$$\hat{c}^- = 1 - r_r\hat{r} - e_r\hat{e} - x_r\hat{x} - p_r\hat{p}, \tag{53}$$

with dimensionless rates

$$\begin{array}{cccc} \hat{r}_s \equiv \hat{e}\frac{\hat{s}}{\hat{K}_s+\hat{s}}\frac{1}{1+\hat{p}/\hat{K}_i}, & \hat{r}_e^+ \equiv \frac{\hat{r}}{\hat{K}_e+\hat{r}}\frac{1+\hat{K}_2\hat{x}^2}{K_3+\hat{K}_2\hat{x}^2}, & \hat{r}_e^- = \hat{k}_e^-\hat{e}, & \hat{r}_r^+ \equiv \hat{k}_r^+\hat{p}\hat{r}, \\ \hat{r}_r^- = \hat{k}_r^-\hat{r}, & \hat{r}_x \equiv \hat{x}, & \hat{r}_{\mathrm{co}_2} \equiv \hat{p}, & \hat{r}_c^+ \equiv \hat{r}\frac{\hat{p}}{\hat{K}_c+\hat{p}}, \\ & \hat{r}_c^- \equiv \hat{k}_c^-\hat{c}^-, & \hat{r}_g \equiv \hat{r}_s - \hat{r}_{\mathrm{co}_2}, & \end{array}$$

and dimensionless parameters

$$\begin{array}{ccccccc} \hat{D} \equiv Dt_r, & \hat{K}_s \equiv \frac{K_s}{s_r}, & \hat{K}_i \equiv \frac{K_i}{p_r}, & \hat{K}_e \equiv \frac{K_e}{r_r}, & \hat{K}_2 \equiv K_2x_r^2, & \hat{k}_e^- \equiv k_e^-t_r, \\ \hat{k}_r^+ \equiv \frac{k_r^+}{k_{\mathrm{co}_2}}, & \hat{k}_r^- \equiv k_r^-t_r, & \tau_x \equiv \frac{1}{k_xt_r}, & \tau_p \equiv \frac{1}{k_{\mathrm{co}_2}t_r}, & \hat{K}_c \equiv \frac{K_c}{p_r}, & \hat{k}_c^- \equiv k_c^-t_r. \end{array}$$

The quasi-steady-state assumption implies that $\tau_x, \tau_p, e_r, x_r, p_r \ll 1$. Hence, equations (51–53) can be approximated with

$$\begin{aligned} 0 &\approx \hat{r}_s - \hat{r}_x, \\ 0 &\approx \hat{r}_x - \hat{r}_{\mathrm{co}_2} - \left(\hat{r}_c^+ - \hat{r}_c^-\right) - r_r\left(\hat{r}_r^+ - \hat{r}_r^-\right), \\ 1 &\approx \hat{c}^- + r_r r. \end{aligned}$$

It follows from the first two equations that

$$\hat{r}_g \equiv \hat{r}_s - \hat{r}_{\mathrm{co}_2} \approx \left(\hat{r}_c^+ - \hat{r}_c^-\right) + r_r\left(\hat{r}_r^+ - \hat{r}_r^-\right).$$

In other words, X and P rapidly achieve quasi-steady state, and the specific growth rate during the subsequent motion is effectively the sum of the net specific protein and RNA synthesis rates. Thus, we arrive at the equations

$$\begin{aligned} \frac{d\hat{s}}{d\hat{t}} &= \hat{D}(1-\hat{s}) - \hat{r}_s\hat{c}, \\ \frac{d\hat{c}}{d\hat{t}} &= \left(\hat{r}_g - \hat{D}\right)\hat{c}, \\ \frac{d\hat{e}}{d\hat{t}} &= \hat{r}_e^+ - \hat{r}_e^- - \hat{r}_g\hat{e}, \\ \frac{d\hat{r}}{d\hat{t}} &= \hat{r}_r^+ - \hat{r}_r^- - \hat{r}_g\hat{r}, \\ 0 &\approx \hat{r}_s - \hat{r}_x, \\ 0 &\approx \hat{r}_x - \hat{r}_{\mathrm{co}_2} - r_g, \\ \hat{c}^- &\approx 1 - r_r\hat{r}. \end{aligned}$$

The reduced equations (19–25) are obtained from these equations by reverting to the original (dimensional) variables. This quasi-steady state is well defined, because the approximate "slow" manifold is unique and globally attracting. To see this, consider the approximate "fast" equations

$$\dot{x} = \frac{V_s e\ \sigma(s)}{1+\frac{p}{K_i}} - k_x x, \tag{54}$$

$$\dot{p} = k_x x - k_{co_2} p - V_c r\frac{p}{K_c+p} - k_r^+ rp + k_r^- r + k_c^- c^-, \tag{55}$$

and treat the variables $s,\ e,\ r,\ c^- > 0$ as (slowly varying) parameters. Then it follows that

1. If $x = 0$ and $p \geq 0$, then $\dot{x} > 0$ due to (54). If $p = 0$ and $x \geq 0$, then $\dot{p} > 0$ due to (55). Hence both x and p remain strictly positive at all times.
2. If $p \geq 0$ and x becomes too large, namely, if $x > \frac{V_s e\sigma}{k_x}$, then $\dot{x} < 0$ due to (54). Hence, x remains bounded at all times. Since x remains bounded, equation (55) implies that p also remains bounded.
3. For any combination $s,\ e,\ r,\ c^- > 0$, the Jacobian of (54–55) has the form

$$J = \frac{\partial(\dot{x},\dot{p})}{\partial(x,p)} = \begin{pmatrix} - & - \\ + & - \end{pmatrix}. \tag{56}$$

   This observation implies that
   (a) Since the divergence of (54–55) (equivalently, the trace of J) is negative for all $x,\ p \geq 0$, the system (54–55) cannot have periodic solutions. Since all positive solutions are bounded, every positive solution must converge

to a steady state. In addition, the signs of the off-diagonal entries of J are such that the orbits in the (x, p) plane rotate counterclockwise.

(b) At any steady state of (54–55), we have that $\operatorname{tr} J < 0$ and $\det J > 0$. Thus all steady states must be stable. Therefore, only one positive steady state of (54–55) must exist.

We conclude that for any combination $s,\ e,\ r,\ c^- > 0$, the fast system (54–55) admits a unique globally attracting quasi-steady state $(\overline{x}, \overline{p})$. Hence, the QSSA is well defined for all $s,\ e,\ r,\ c^- > 0$.

REFERENCES

[1] R. Aris and A. E. Humphrey (1977), Dynamics of a chemostat in which two organisms compete for a common substrate, Biotechnol. Bioeng. 19, 1375–1386.

[2] F. Azam and A. Z. Worden (2004), Microbes, molecules, and marine ecosystems, Science 303, pp. 1622–1624.

[3] T. K. N. Baidya, F. C. Webb, and M. D. Lilly (1967), Utilization of mixed sugars in continuous fermentation. I., Biotechnol. Bioeng. 9, 195–204.

[4] M. Bally and T. Egli (1996), Dynamics of substrate consumption and enzyme synthesis in *Chelatobacter heintzii* during growth in carbon-limited continuous culture with different mixtures of glucose and nitrilotriacetic acid (NTA), Appl. Environ. Microbiol. 62, 133–140.

[5] M. M. Ballyk and G. S. K. Wolkowicz (1993), Exploitative competition in the chemostat for two perfectly substitutable resources, Math. Biosci. 118, 127–180.

[6] B. C. Baltzis and A. G. Frederickson (1988), Limitation of growth rate by two complementary nutrients, Biotechnol. Bioeng. 31, 75–86.

[7] J. R. Beckwith and D. Zipser, The Lactose Operon, Cold Spring Harbor Laboratory, 1970.

[8] H. Bremer and P. P. Dennis (1975), Transition period following a nutritional shift-up in the bacterium *Escherichia coli* B/r: Stable RNA and protein synthesis, J. Theor. Biol. 52, 365–382.

[9] U. Brinkmann and W. Babel (1992), Simultaneous utilization of heterotrophic substrates by Hansenula polymorpha MH30 results in enhanced growth rates, App. Microbiol. Biotechnol. 37, 98–103.

[10] G. J. Butler and G. S. K. Wolkowicz (1985), Exploitative competition in a chemostat for two complementary, and possibly inhibitory, resources, Math. Biosci. 83, 1–48.

[11] M. Cohn and K. Horibata (1959), Inhibition by glucose of the induced synthesis of the β-galactoside-enzyme system of *Escherichia coli*. Analysis of maintenance, J. Bacteriol. 78, 601–602.

[12] C. L. Cooney, D. I. C. Wang, and R. I. Mateles (1976), Growth of *Aerobacter aerogenes* in a chemostat with double nutrient limitations, Appl. Environ. Micorbiol. 31, 91–98.

[13] P. De Leenheer, S. A. Levin, E. D. Sontag, and C. A. Klausmeier (2003), Global stability in a chemostat with multiple nutrients, DIMACS technical report 2003-40.

[14] M. R. Droop (1974), The nutrient status of lagal cells in continuous culture, J. Mar. Biol. Assoc. UK 48, 689–733.

[15] M. R. Droop (1983), Twenty-five years of algal growth kinetics, a personal view, Botan. Mar. 26, 99–112.

[16] R. Durner, B. Witholt, and T. Egli (2000), Accumulation of poly[(R)-3-hydroxyalkanoates] in *Pseudomonas oleovarans* during growth with octanoate in continuous culture at different dilution rates, Appl. Env. Microbiol. 66, 3408–3414.

[17] R. Durner, M. Zihn, B. Witholt, and T. Egli (2001), Accumulation of poly[(R)-3-hydroxyalkanoates] in *Pseudomonas oleovarans* during growth in batch and continuous culture with different carbon sources, Biotechnol. Bioeng. 72, 278–288.

[18] T. Egli, O. Käppeli, and A. Fiechter (1982), Mixed substrate growth of methylotrophic yeasts in chemostat culture: Influence of dilution rate on the utilization of a mixture of methanol and glucose, Arch. Microbiol. 131, 8–13.

[19] T. Egli, N. D. Lindley, and J. R. Quayle (1983), Regulation of enzyme synthesis and variation of residual methanol concentration during carbon-limited growth of *Kloeckera sp.* on mixtures of methanol and glucose, J. Gen. Microbiol. 129, 1269–1281.

[20] T. Egli, C. Bosshard, and G. Hamer (1986), Simultaneous utilization of methanol-glucose mixtures by Hansenula polymorpha in chemostat: Influence of dilution rate and mixture composition on utilization pattern, Biotechn. Bioeng. 28, 1735–1741.
[21] T. Egli (1995), The ecological and physiological significance of the growth of heterotrophic microorganisms with mixtures of substrates, Adv. Microbiol. Ecol. 14, 305–386.
[22] A. G. Frederickson and G. Stephanopoulos (1981), Microbial competition, Science 213, 972–979.
[23] M. E. Gilpin and K. E. Justice (1972), Nature 236, 273.
[24] S. Gupta, S. S. Pilyugin, and A. Narang, Dynamics of single-substrate cultures: The role of ribosomes, J. Theor. Biol., in press.
[25] S. R. Hansen and S. P. Hubbell (1980), Single nutrient competiton: agreement between experimental and theoretical forecast outcomes, Science 207, 1491–1493.
[26] D. E. F. Harrison and H. H. Topiwala (1974), Transient and oscillatory states of continuous culture, Adv. Biochem. Eng. 3, 167–219.
[27] M. J. Harte and F. C. Webb (1967), Utilization of mixed sugars in continuous fermentation. II., Biotechnol. Bioeng. 9, pp. 205-221.
[28] R. J. Harvey (1970), Metabolic regulation in glucose-limited chemostat cultures of *Escherichia coli*, J. Bacteriol. 104, 698–706.
[29] S. B. Hsu, S. P. Hubbell, and P. Waltman (1977), A mathematical theory for single nutrient competition in continuous cultures of micro-organisms, SIAM J. Appl. Math. 32, 366–383.
[30] S. B. Hsu (1978), Limiting behavior for competing species, SIAM J. Appl. Math. 34, 760–763.
[31] S. B. Hsu, K. S. Cheng, and S. P. Hubbell (1981), Exploitative competition of microorganism for two complementary nutrients in continuous culture, SIAM J. Appl. Math. 41, 422–444.
[32] D. Herbert, R. Elsworth, and R. C. Telling (1956), The continuous culture of bacteria: A theoretical and experimental study, J. Gen. Microbiol. 14, 601–622.
[33] K. F. Jensen and S. Pedersen (1990), Metanolic growth rate control in *Escherichia coli* may be a consequence of subsaturation of the macromolecular biosynthetic apparatus with substrates and catalytic components, Microbiol. Rev. 54, 89–100.
[34] C. A. Klausmeier, E. Litchman, and S. A. Levin, Phytoplankton growth and stoichiometry under multiple nutrient limitation. Limnol. Ocean., in press.
[35] S. Koga and A. E. Humphrey (1967), Study of the dynamic behavior of the chemostat system, Biotechnol. Bioeng. 9, 375–386.
[36] K. Kovarova, A. Kach, V. Chaloupka, and T. Egli (1996), Cultivation of Escherichia coli with mixtures of 3-phenylpropionic acid and glucose, Biodegradation, 7, 445–453.
[37] K. Kovarova-Kovar and T. Egli (1998), Growth kinetics of suspended microbial cells: From single substrate-controlled growth to mixed-substrate kinetics, Microbiol. Mol. Biol. Rev. 62 (3), 646–666.
[38] T. Legovic and A. Cruzado (1997), A model of phytoplankton growth on multiple nutrients based on the Michaelis-Menten-Monod uptake, Droop's growth and Liebig's law, Ecol. Model. 99, 19–31.
[39] U. Lendenmann, M. Snozzi, and T. Egli (1992), Simultaneous utilization of diauxic sugar mixtures by *Escherichia coli*, 6th International Symposium on Microbial Ecology, Abstracts, p. 254.
[40] J. A. Leon and D. B. Tumpson (1975), Competition between two species for two complementary or substitutable substrates, J. Theor. Biol. 50, 185–201.
[41] J. Monod (1942), Recherches sur la croissance des cultures bacteriennes, Actualites Scientifique et Industrielles 911, p. 1-215.
[42] J. D. Murray, Mathematical Biology, Biomethematics Texts, Springer-Verlag, New York, 1989.
[43] S. Nagai, Y. Nishizawa, I. Endo, and S. Aiba (1968), Response of a chemostatic culture of *Azotobacter vinelandii* to a delta type pulse of glucose, J. Gen. Appl. Microbiol. 14, 121–134.
[44] A. Narang, A. Konopka, and D. Ramkrishna (1997), The dynamics of microbial growth on mixtures of substrates in batch reactors, J. Theor. Biol. 184, 301–317.
[45] A. Narang, A. E. Konopka, D. Ramkrishna (1997), New patterns of mixed-substrate utilization during batch growth of *Escherichia coli* K12. Biotech. Bioeng. 55, 747–757.
[46] A. Narang (1998), The dynamical analogy between microbial growth on mixtures of substitutable substrates and population growth of competing species, Biotech. Bioeng. 59, 116–121.
[47] A. Narang (1998), The steady states of microbial growth on mixtures of substitutable substrates in a chemostat, J. Theor. Biol. 190, 241–261.

[48] F. C. Neidhardt, J. L. Ingraham, and M. Schaechter, Physiology of the Bacterial Cell: A Molecular Approach, Frank Sinauer Associates, Sunderland, Massachusetts, 1990.
[49] O. M. Neijssel, S. Hueting, and D. W. Tempest (1977), Glucose transport capacity is not the rate-limiting step in the growth of some wild-type strains of *Escherichia coli* and *Klebsiella aerogenes* in chemostat culture, FEMS Microbiol. Lett. 2, 1–3.
[50] J. Nielsen and J. Villadsen (1992), Modeling of microbial kinetics, Chem. Eng. Sci. 47, pp. 4225–4270.
[51] R. W. O'Brien, O. M. Neijssel, and D. W. Tempest (1980), Glucose phosphoenolpyruvate phosphotransferase activity and glucose uptake rate of *Klebsiella aerogenes* growing in a chemostat culture, J. Gen. Microbiol. 116, 305–314.
[52] S. S. Pilyugin, G. T. Reeves, and A. Narang, Predicting stability of mixed microbial cultures from single species experiments: 1. Phenomenological model, in press.
[53] S. S. Pilyugin, G. T. Reeves, and A. Narang, Predicting stability of mixed microbial cultures from single species experiments: 2. Physiological model, in press.
[54] S. S. Pilyugin and P. Waltman (2003), Multiple limit cycles in the chemostat with variable yield, Math. Biosci. 182, 151–166.
[55] E. O. Powell (1958), Criteria for growth of contaminants and mutants in continuous culture, J. Gen. Microbiol. 18, 259–268.
[56] G. T. Reeves, A. Narang, and S. S. Pilyugin (2004), Growth of mixed cultures on mixtures of substitutable substrates: The operating diagram for a structured model, J. Theor. Biol. 226, 143–157.
[57] J. Shoemaker, G. T. Reeves, S. Gupta, S. S. Pilyugin, T. Egli, and A. Narang (2003), The dynamics of single-substrate continuous cultures: The role of transport enzymes, J. Theor. Biol. 222, 307–322.
[58] H. L. Smith and P. Waltman, The Theory of the Chemostat, Cambridge University Press, Cambridge, UK, 1995.
[59] D. W. Tempest, D. Herbert, and P. J. Phipps, Studies on the growth of *Aerobacter aerogenes* at low dilution rates in a chemostat, In *Microbial Physiology and Continuous Culture*, pp. 240–253, HMSO, London, 1967.
[60] H. R. Thieme (1994), Asymptotically autonomous differential equations in the plane, Rocky Mount. J. Math. 24, 351–380.
[61] D. Tilman (1980), Resources: a graphical-mechanistic approach to competition and predation, Am. Nat. 116 (3), 362–393.
[62] D. Tilman, Resource Competition and Community Structure, Princeton University Press, 1982.
[63] A. J. Watson and J. C. Orr, Carbon dioxide fluxes in the ocean. In: *Ocean biogeochemistry* (M. J. R. Fasham, Ed.), Chapter 5, pp. 123-141, Springer-New York, 2003.
[64] G. S. Wolkowicz and Z. Lu (1992), Global dynamics of a mathematical model of competition in the chemostat: General response functions and differential death rates, SIAM J. Appl. Math. 52, 222–233.
[65] H. S. Yun, J. Hong, and H. C. Lim (1996), Regulation of ribosome synthesis in *Escherichia coli*: Effects of temperature and dilution rate changes, Biotechnol. Bioeng. 52, 615–624.
[66] M. L. Zeeman (1993), Hopf bifurcations in competitive three-dimensional Lotka-Volterra systems, Dyn. Stab. Sys. 8(3), 189–217.
[67] X. Zhang, P. Dennis, M. Ehrneberg, and H. Bremer (2002), Kinetic properties of *rrn* propmoters in *Escherichia coli*, Biochimie 84, 981–996.

Received on Sept. 2, 2004. Revised on Oct. 21, 2004.

E-mail address: anarang@che.ufl.edu
E-mail address: pilyugin@math.ufl.edu